ADVANCED FUNCTIONAL MATERIALS
www.afm-journal.de

Recent Progress in Liquid Crystal Elastomer Actuators: Mechanisms, Fabrication, and Multifunctional Applications

*Chenglin Li, Jing Li, Huiling Duan, and Xin Yi**

Liquid crystal elastomers (LCEs) uniquely couple the anisotropic ordering of liquid crystal (LC) phases with the elasticity of polymer networks, enabling large, reversible, and programmable deformations under diverse stimuli, including light, heat, electric and magnetic fields, humidity, and pneumatic pressure. These capabilities place LCEs at the forefront of next-generation responsive materials. Recent years have witnessed a surge of interest in LCE-based actuators, fueled by their promise in robotics, artificial muscles, adaptive textiles, self-sensing platforms, and medical devices. This review provides a comprehensive overview of recent progress in LCE research, emphasizing fundamental actuation mechanisms, innovative fabrication strategies, and their implementation in cutting-edge applications. The performance of LCE actuators is critically assessed across a range of application scenarios, highlighting key parameters such as strain magnitude, response time, and energy efficiency. Finally, current challenges–ranging from materials integration and long-term durability to multifunctional system design–are examined, and promising future directions are outlined to unlock the full potential of LCE actuators in real-world applications.

1. Introduction

The rapid advancement of smart materials has unlocked a diverse array of applications across robotics, artificial muscles, smart textiles, self-sensing devices, flexible electronics, and biomedical technologies.[1–7] These materials are characterized by their multi-stimuli responsiveness, reversible deformation capabilities, biocompatibility, and multifunctionality. Currently, the spectrum of smart materials encompasses hydrogels,[8–10] shape memory alloys and polymers,[11–13] LCEs,[14,15] dielectric elastomers,[16–19] and magnetic composites,[20–22] among others. Among these, LCEs stand out for their ability to achieve large, reversible deformations—up to ≈80%—with relatively fast response times compared to many alternatives.[23] These characteristics, combined with their programmability, excellent processability, and responsiveness to diverse external stimuli—including electric and magnetic fields, heat, light, humidity, and pneumatic pressure—have driven intense research attention in recent years.[24–31]

The reversible deformation behavior of LCEs originates from the unique capability of LC mesogens to transition between ordered (nematic) and disordered (isotropic) states during phase transitions. In thermally responsive systems, LC mesogens exhibit nematic order below the nematic-to-isotropic transition temperature (T_{NI}).[32,33] Upon heating above T_{NI}, the mesogens undergo a phase transition to the isotropic state, disrupting the anisotropic order of the polymer network. This molecular rearrangement induces a macroscopic contraction of the elastomer along the initial director axis.

Building on their outstanding actuation capabilities, LCEs have been extensively developed as soft actuators across diverse fields. They combine high flexibility, environmental compatibility, adaptability, structural simplicity, and operational safety—features difficult to achieve with conventional rigid actuators.[34,35] The excellent processability of LCEs enables fabrication into varied architectures, facilitating integration into functional systems. Through rational design and advanced fabrication techniques—including molding,[36–38] spinning,[39,40] and printing[41–47]—LCEs have been engineered into increasingly complex hierarchical structures[48–50] with programmable actuation. These architectures can be classified by dimensionality: 0D particles[51–53] exhibit multi-responsive deformations and motions at the submillimeter scale, enabling expanded opportunities for precise manipulation and transport of microscopic objects; 1D fibers[54–56] mimicking natural muscles, provide rapid, anisotropic responses for artificial muscles and wearable devices; 2D thin films[57–64] allow programmable bending, twisting, and folding for soft robots and adaptive grippers; 3D structures,[65–67] fabricated via molding or additive manufacturing, enable macroscale integration, complex shape morphing, and programmable anisotropy. Interdisciplinary efforts spanning materials science, chemistry, engineering, computer science, and biomedicine[68–70] have further enhanced LCE performance and versatility, expanding their applications and accelerating translation from laboratory research to real-world deployment.

To build on recent advances in materials development and application strategies, this review systematically summarizes the

C. Li, J. Li, H. Duan, X. Yi
School of Mechanics and Engineering Science
Peking University
Beijing 100871, China
E-mail: xyi@pku.edu.cn

The ORCID identification number(s) for the author(s) of this article can be found under https://doi.org/10.1002/adfm.202514063

DOI: 10.1002/adfm.202514063

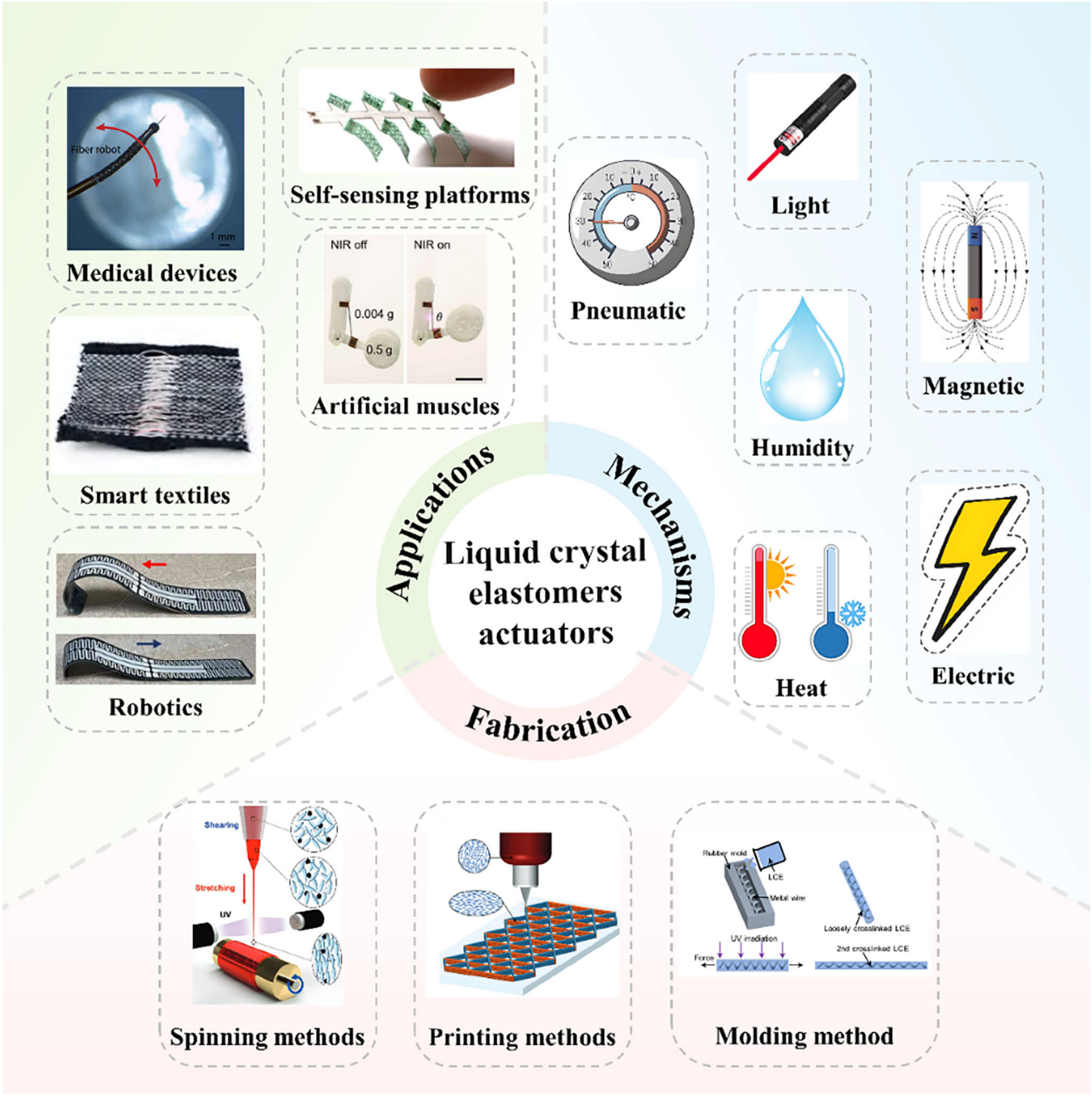

Figure 1. Schematic overview of the actuation mechanisms, fabrication methods, and application domains of the LCE actuators. Representative fabrication techniques include molding (Reproduced with permission.[71] Copyright 2021, American Association for the Advancement of Science (AAAS)), printing (Reproduced with permission.[72] Copyright 2024, Wiley-VCH), and spinning (Reproduced with permission.[73] Copyright 2023, Wiley-VCH). Application areas encompass robotics (Reproduced with permission.[74] Copyright 2023, AAAS), artificial muscles (Reproduced with permission.[75] Copyright 2021, AAAS), smart textiles (Reproduced with permission.[76] Copyright 2023, Association for Computing Machinery (ACM)), self-sensing platforms (Reproduced with permission.[77] Copyright 2024, Springer Nature), and medical devices (Reproduced with permission.[5] Copyright 2024, AAAS).

latest progress in LCE-based actuators, as outlined in **Figure 1**. Section 2 discusses the fundamental actuation mechanisms of LCEs under diverse external stimuli—including heat, pneumatic pressure, light, magnetic fields, humidity, and electric fields—highlighting how these interactions drive macroscopic shape transformations. Section 3 reviews state-of-the-art fabrication techniques, including synthesis, spinning, molding, and printing, with a critical comparison of their respective advantages and limitations. Section 4 explores the integration of LCE actuators into functional systems, focusing on applications in

robotics, artificial muscles, smart textiles, medical devices, and self-sensing platforms. Finally, we highlight key challenges to practical deployment and propose future directions to advance actuation performance, scalable manufacturing, and multifunctional integration, thereby providing a cohesive outlook for the next generation of LCE-based soft actuators.

2. Actuation Mechanisms of LCE Actuators

LCE actuators demonstrate exceptional reversible deformation capabilities driven by the dynamic reorientation of LC mesogens. Under external stimuli such as electric,[78–82] magnetic fields,[31,83,84] heat,[85–87] light,[88–91] pneumatic pressure,[92,93] or humidity,[25,31,94,95] the mesogens undergo a nematic-to-isotropic transition, losing their orientational order. Although the mesogens themselves become disordered, the polymer network retains the anisotropy imposed during crosslinking. As a result, the network contracts preferentially along the original mesogen alignment direction, producing macroscopic shape change. Removing the stimulus restores mesogen alignment, enabling fast and reversible actuation cycles.[96–99] Beyond thermal actuation, pneumatic responsiveness leverages the intrinsic softness of LCEs, while magnetic actuation is achieved by embedding magnetic nanoparticles into the polymer matrix. These approaches expand the multi-stimuli responsiveness of LCEs, allowing activation methods to be tailored to specific applications (**Table 1**). With this versatility, high reversibility, and favorable mechanical properties, LCEs have emerged as key enablers in robotics, artificial muscles, smart textiles, and self-sensing systems.

Thermally induced actuation via direct heating is one of the most fundamental and widely adopted strategies for triggering LCE deformation. As shown in **Figure 2A**, a 3D-printed LCE actuator undergoes pronounced contraction when heated from 30 to 90 °C.[100] This response originates from the temperature-driven nematic-to-isotropic phase transition of aligned LC mesogens, which disrupts molecular order and produces macroscopic deformation of the elastomer. The process is reversible, highlighting the ability of LCEs to convert thermal energy into mechanical work. Actuation performance can be tuned through ambient temperature, heating duration, and heating location. Global heating, for example with a hot plate, produces large-scale, repeatable deformations with high controllability, suitable for soft robots and deployable structures. Yet it requires uniform heating and cannot achieve spatial selectivity. Localized heating instead enables programmable responses, offering opportunities for adaptive devices, micromanipulation, and functional surfaces. Combining molecular alignment with structural design further expands multimodal thermoresponsive behaviors.[85–87] A remaining challenge, however, is the slow cooling process, which restricts actuation frequency and hinders use in intelligent systems demanding high speed, resolution, and energy efficiency.

To address the spatial and control limitations of direct thermal heating, light actuation offers a non-contact, localized alternative for actuating LCEs. Incorporating photothermal agents—such as candle soot,[101] gold nanorods,[102] carbon nanotubes (CNTs),[42,103] or semiconductor compounds[36]—into the LCE matrix (Figure 2B) enables efficient light-to-heat conversion. Upon irradiation at suitable wavelengths, these agents absorb light and dissipate it as heat via non-radiative relaxation, generating localized temperature rises that trigger nematic-to-isotropic transitions and region-specific deformation.

Beyond photothermal approaches, LCEs can be rendered intrinsically light-responsive by integrating photoisomerizable moieties such as azobenzene.[104] These molecules undergo reversible trans–cis isomerization under UV or visible light (Figure 2C). When aligned parallel to LC mesogens, isomerization disrupts molecular order and induces bending toward the light source.[105] If the mesogens are aligned perpendicularly, the isomerization generates anisotropic stress in the orthogonal direction, resulting in bending away from the light.[106]

Light-driven LCE actuators offer several key advantages, including high spatial resolution, precise controllability, and non-contact operation,[104,107] making them attractive for applications in soft robotics, microfiber robots, and programmable morphing. Their performance, however, can be limited by light penetration depth, irradiation uniformity, photothermal efficiency, and slow cooling, while reliance on functional dopants or chromophores adds material complexity.

Electromagnetic induction heating provides another non-contact strategy. For instance, LCEs embedded with conductive materials can be actuated via inductive heating under alternating magnetic fields.[108] In this method, the oscillating magnetic field induces eddy currents within conductive inclusions, generating internal heat that raises the local temperature of the LCE. Once the temperature exceeds the phase transition threshold, the LC mesogens transition from an ordered to an isotropic state, prompting macroscopic deformation (Figure 2D). This wireless heating approach enables remote actuation in enclosed or hard-to-access environments and is promising for soft robotics. Nonetheless, its relatively low spatial precision and bulky electromagnetic setups pose challenges for finely controlled or portable systems.

Joule heating by contrast provides a direct and widely adopted method for LCE actuation (Figure 2E). Conductive materials—such as metal wires,[37,71,109,110] liquid metals,[56,57,111] CNTs,[112,113] or MXenes[113–115]—embedded or patterned within the LCE generate heat via resistive losses when an electric current is applied, triggering nematic-to-isotropic transitions and enabling rapid, uniform deformation. This approach offers precise control through current or voltage modulation and integrates easily with electrical circuits, making it well suited for smart wearables, robotics, and human–machine interfaces. Its scalability and responsiveness make it an attractive choice for developing next-generation intelligent actuation systems with enhanced programmability and multifunctionality.

In addition to thermally and light-driven mechanisms, LCE actuators can respond to other stimuli, broadening their functional versatility. For example, pneumatic actuation can be achieved by engineering hollow LCE fibers, where controlled air pressure induces radial expansion and axial contraction, enabling large, rapid shape changes (Figure 2F).[92] This makes them well suited for bioinspired morphing structures and soft robotic systems that require high compliance and adaptability. However, reliance on pumps, valves, and tubing limits integration and miniaturization, while air compressibility and the nonlinear response of hollow chambers reduce control precision.

Magnetic actuation is another effective strategy, realized by incorporating magnetic particles—such as Fe_3O_4 or NdFeB—into

Table 1. Summary and comparison of LCE actuators under different actuation mechanisms.

Actuation mechanisms		Features	Advantages	Limitations	Response Time	Applications	Refs.
Thermal	Environmental	Direct heating induces nematic–isotropic transition	Simple implementation	Slow actuation, low spatial precision, external thermal control required	Slow (≈10 s–min)	Soft actuators, smart structures	[85–87,100,120]
	Photothermal	Light-to-heat conversion triggers actuation	Localized control, non-contact, high spatial resolution	Requires external light source, risk of thermal accumulation	Fast–Moderate (≈0.15–10 s)	Artificial muscles, soft actuators	[36,42,88,101–103]
	Electromagnetic-induced	Electromagnetic induction heating	Wireless actuation, fast response, suitable for enclosed environments	Complex magnetic setup, limited spatial precision	Fast (≈1 s)	Wireless soft robotics	[108,121]
	Electrothermal	Actuation via resistive heating	Precise control, easy integration with electronics	Requires embedded electrodes, fabrication complexity, power consumption	Fast–Moderate (≈0.12–10 s)	Smart wearables, soft robotics, human–machine interfaces	[37,78–82]
Light-responsive		Trans–cis isomerization of azobenzene moieties	High spatial resolution, remote and precise control	Specific light source requirements, limited penetration depth	Fast–Moderate (≈1–10 s)	Light-driven microactuators, fiber robots	[89,90,104–106,122]
Pneumatic		Shape change via pneumatic inflation or pressure	High force output, rapid response	Requires bulky external equipment, tubing or wiring required	Fast–Moderate (≈0.8–5 s)	Artificial muscles, soft grippers	[92,93]
Magnetic		Embedded materials respond to external magnetic fields	Remote actuation, compatible with multiple stimuli, high spatial precision	Requires strong magnetic fields, complex setups, low spatial resolution	Fast (≈0.4–3 s)	Biomedical devices, wireless soft robots	[31,83,94,116]
Humidity		LC network swells under humid conditions	No external energy source required, structurally simple	Low actuation precision, slow response, limited force output	Slow (≈1 min)	Soft actuators, sensors	[25,31,94,95]

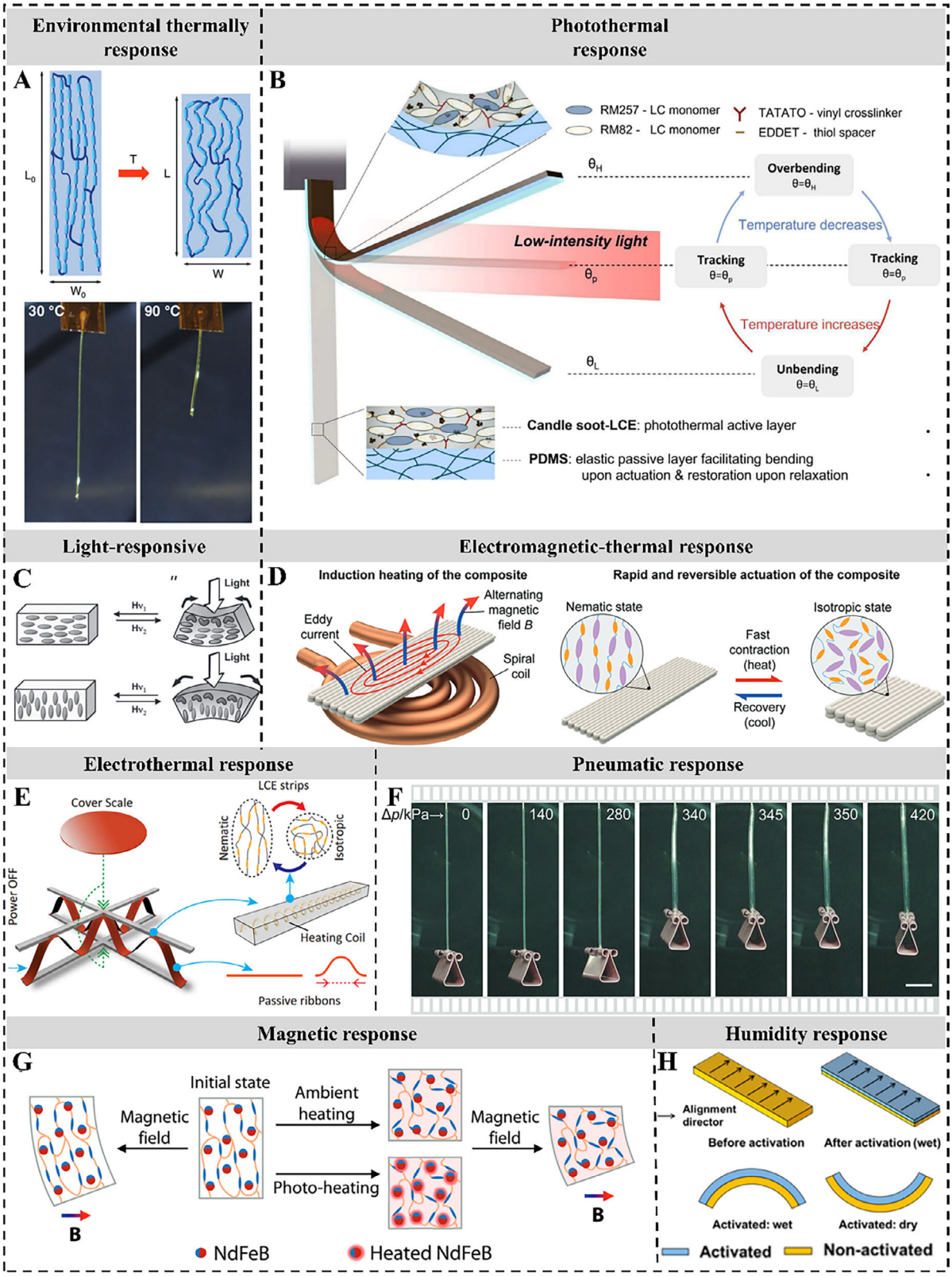

the LCE matrix, enabling remote, non-contact control of deformation (Figure 2G).[83,116] This approach expands the operational flexibility of LCE-based devices. However, it suffers from low spatial resolution due to rapid decay of magnetic field strength, and aggregation of embedded magnetic fillers can compromise material uniformity, actuation performance, and long-term durability.

Humidity-responsive LCEs undergo reversible swelling and deswelling in response to environmental humidity, enabling repeated and controllable dynamic deformations. Unlike light-, electric-, magnetic-, or thermally driven LCEs, they require no external energy, relying on water absorption to expand the LC network and induce bending or other shape changes (Figure 2H).[25] This passive actuation provides structural simplicity, adaptive responses, and excellent compliance, making them suitable for soft actuators and sensors. However, slow water diffusion limits actuation speed and precision, restricting their use in high-power or high-accuracy applications.

Advancing LCE actuation requires balancing efficiency, spatial precision, and system complexity. Innovations in material design, composites, and structural fabrication will be key to overcoming current limitations. Together, these alternative mechanisms expand LCE functionality and provide a versatile platform for next-generation applications in flexible robotics, artificial muscles, smart textiles, and self-sensing systems.

3. Fabrication Methods of LCEs

LCEs offer excellent processability, enabling diverse geometries for functional applications. Their chemical synthesis route strongly influences molecular architecture, crosslinking density, and compatibility with different processing strategies. Key fabrication techniques include spinning, molding, and printing, each with distinct advantages and limitations (**Table 2**). This section summarizes their principles, processes, and trade-offs, offering guidance on suitable application scenarios.

3.1. Synthetic Strategies of LCEs

LCEs, intelligent soft materials that couple LC anisotropy with polymer elasticity, show properties strongly governed by chemical synthesis and processing strategies. Recently, click reactions—including thiol–ene/yne, aza-Michael, and thiol–Michael additions—have become central to LCE design owing to their efficiency, mild conditions, and high selectivity. Thiol–ene/yne reactions proceed via a free-radical step-growth mechanism, rapidly forming uniform cross-linked networks with low shrinkage, fast reaction kinetics, and high homogeneity.[117] These merits have enabled their wide use in both main-chain and side-chain LCEs, as well as facile macroscopic alignment under external fields (e.g., magnetic fields, shear flow) and compatibility with microfluidic or molding techniques.[118,119]

Aza–Michael addition, where nitrogen nucleophiles (e.g., amines) attack the β-carbon of α,β-unsaturated carbonyls to form carbon–nitrogen bonds, offers mild conditions, suitable kinetics, and high conversion efficiency, allowing sufficient time for mesogen alignment in low-viscosity systems.[66,123] This strategy is further compatible with surface alignment and advanced approaches such as 4D printing and photopolymerization, imparting programmability and enabling architecturally complex LCE structures.

Thiol–Michael addition enables controlled LCE network construction through the nucleophilic addition of thiols to electron-deficient alkenes such as acrylates.[124–126] Typically, a two-step strategy is adopted: a low-crosslinking pregel is first formed to allow LC mesogen alignment, followed by secondary crosslinking to lock the ordered structure, yielding LCEs with stable actuation performance. This method offers fast kinetics, mild conditions, and excellent tunability, permitting precise control over crosslinking density and incorporation of functional groups for light responsiveness or mechanochromism. As a result, thiol–Michael addition is widely employed for synthesizing functional LCEs and designing high-performance actuators.

More broadly, click reactions–valued for their simplicity, rapid kinetics, and scalability–have expanded the versatility of LCEs. Their integration with emerging 3D and 4D printing techniques enables programmable deformation and complex actuation, advancing applications in soft robotics, bioinspired actuators, and wearable optical systems, and laying the foundation for a shift from responsive to adaptive materials.

3.2. Spinning Methods

Spinning techniques for LCE fabrication are generally classified into melt spinning, wet/dry spinning, and electrospinning.[39,40,75] In these cases, LC precursors are formulated into spin-compatible inks and extruded from a syringe to form fiber-like structures, with alignment controlled by mechanical forces, shear, or electric fields.

In melt spinning, the precursor ink is heated to a molten state to achieve suitable rheology, extruded through a nozzle, and rapidly solidified upon cooling to yield continuous fibers. Mesogen alignment and crosslinking are subsequently tailored to tune mechanical and functional properties. Recent advances combine high-precision extrusion with roller-based collection, enabling uniform fiber production, scalable continuous fabrica-

Figure 2. Representative actuation mechanisms of LCE actuators under various stimuli. A) Thermally induced contraction of a 3D-printed LCE actuator under environmental temperature changes (Reproduced with permission.[100] Copyright 2017, Wiley-VCH). B) Periodic and reversible deformation of an LCE oscillator driven by localized light irradiation via photothermal effects (Reproduced with permission.[101] Copyright 2023, AAAS). C) Directional bending deformation of an LCE actuator triggered by light stimulation (Reproduced with permission.[104] Copyright 2011, Wiley-VCH). D) Rapid thermally induced deformation of an LCE actuator activated by electromagnetic induction heating.(Reproduced with permission.[108] Copyright 2023, Wiley-VCH). E) Contraction deformation of an LCE actuator driven by Joule heating (Reproduced with permission.[37] Copyright 2021, AAAS). F) Controlled pneumatic actuation enabled by a hollow-structured LCE actuator (Reproduced with permission.[92] Copyright 2024, Wiley-VCH). G) Multimodal actuation of an LCE actuator doped with NdFeB microparticles under the combined stimuli of magnetic fields, ambient heat, and photothermal effects (Reproduced with permission.[116] Copyright 2023, Wiley-VCH). H) Bending of a humidity-responsive LCE actuator with mesogens aligned perpendicular to the long axis under partial activation (Reproduced with permission.[25] Copyright 2014, American Chemical Society (ACS)).

Table 2. Summary and comparison of different manufacturing methods for LCE actuators.

Methods		Key process factors	Advantages	Limitations	Precision	Refs.
Spinning methods	Melt spinning	Temperature, ink rheology, extrusion pressure	Continuous production, complex fiber architectures, functional filler integration	Limited micrometer-scale diameter control, precise temperature requirements	Micrometer-scale (≈40 µm)	[55,56,113,127]
	Wet spinning	Coagulation bath chemistry, crosslinking conditions	Rapid production (4500 m h^{-1}), easy to integrate with other materials	Specialized equipment requirements, potential environmental and safety concerns	Micrometer-scale (~30 µm)	[128,129]
	Dry spinning	Ink viscosity, shear stress, collector speed	Very high throughput (8400 m h^{-1}), submicron fiber diamater capability	Requires precise parameter control, material/equipment optimization necessary	Micrometer-scale (≈2.6 µm)	[73,130]
	Electrospinning	Electric field strength, ambient humidity, ink conductivity	Submicron fiber diameter capability	High equipment cost, processing complexity	Micrometer-scale (≈4 µm)	[49,75]
Molding method		Mold design, crosslinking conditions, demolding	Simple setup, low equipment cost, versatile geometries	Batch-based process, risk of structural defects during demolding	Millimeter-scale (> 100 µm–mm)	[54,69,71]
Printing methods	Direct ink writing (DIW)	Nozzle size, ink rheology, printing speed and temperature	High design freedom, tunable anisotropy, fast prototyping, path-independent molecular orientation	Low resolution, anisotropy influenced by printing parameters, surface roughness	Micrometer-scale (≈50–100 µm)	[42,93,131]
	Digital light processing (DLP)	Light intensity, light pulse, layer thickness, resin chemistry	High precision, complex 3D structures	Requires photopolymerizable systems, oxygen sensitivity, expensive setup, the difficulty of mesogen alignment	Micrometer-scale (≈1–10 µm)	[67,132]
Imprinting		LCE precursors confined by micro/nanopatterned molds or photolithographic templates, local mesogen alignment controlled by mold morphology or light field	High resolution, enables diverse/topologically complex structures	Limited by mold/photolithography technology, film thickness usually < 100 µm	Micrometer-scale (≈1–30 µm)	[133,134]
Surface alignment		Alignment layers applied (photoalignment, microstructuring, rubbing), low-viscosity precursor mixtures	Enables complex patterning, precise control of LC orientation	Relatively high cost and complex process, restricted to 2D films	Micrometer-scale (≈30 µm)	[135–137]
Mechanical stretch		Stretch direction, crosslinking density, two-step crosslinking, stretching ratio	Simple operation, low equipment requirements, suitable for large-area films or fibers	Limited in achieving complex or high-resolution alignment patterns, shape strongly coupled with alignment	Millimeter-scale (> 100 µm–mm)	[125,138,139]
Self-assembly		Dopant type and concentration, interfacial conditions, thermal and processing conditions	Simple process without sophisticated equipment, can form multi-domain structures	Poor controllability and reproducibility, limited control over molecular alignment	Micrometer-scale (≈1–10 µm)	[140–142]

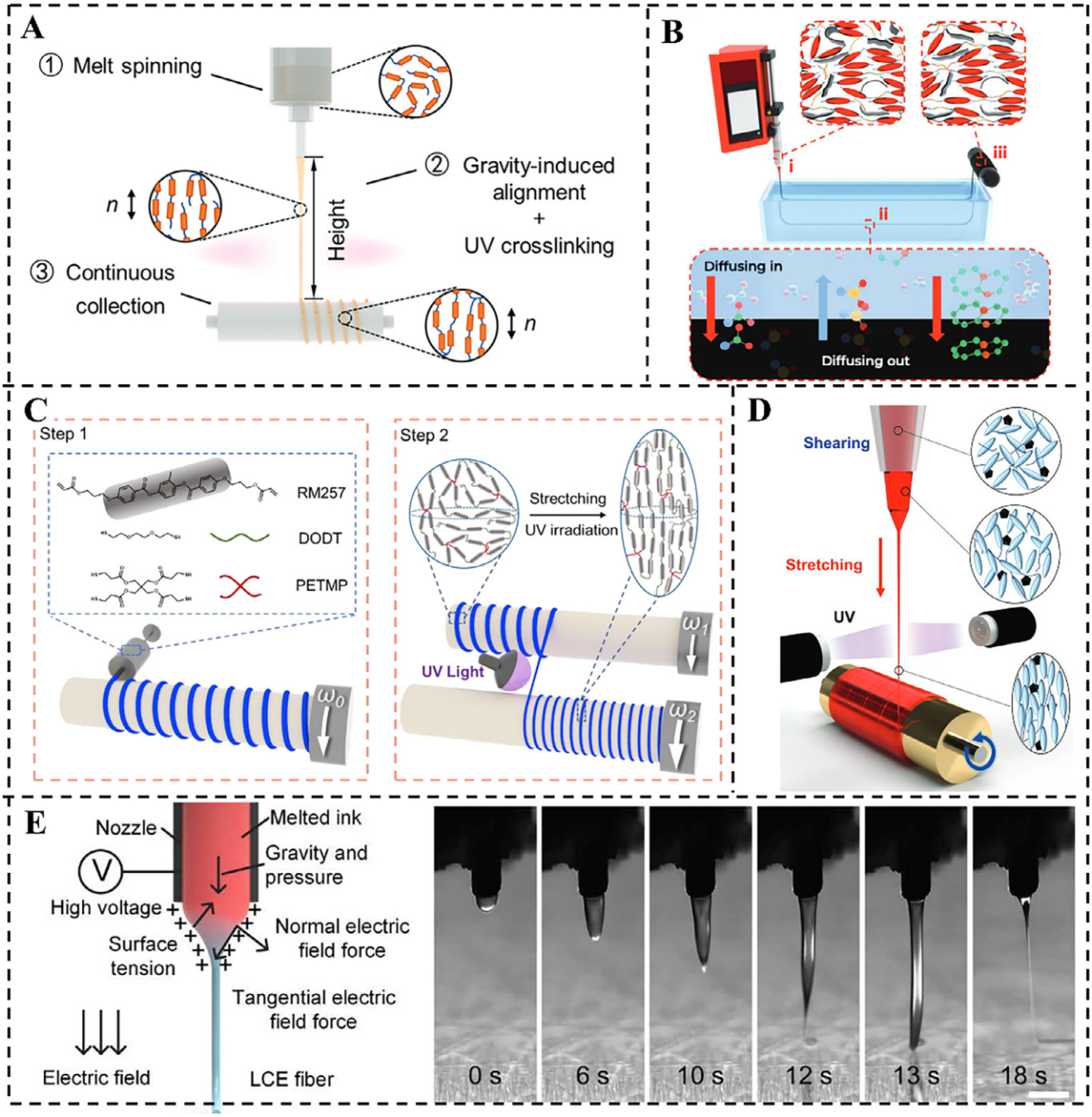

Figure 3. Fabrication of LCE fibers via spinning techniques. A) Schematic of the melt spinning process, where gravity-induced stretching promotes LC mesogen alignment during extrusion (Reproduced with permission.[127] Copyright 2023, Wiley-VCH). B) Illustration of the wet spinning method utilizing a dual-diffusion crosslinking mechanism to rapidly solidify and stabilize LCE fibers (Reproduced with permission.[128] Copyright 2024, Wiley-VCH). C,D) Schematics of dry spinning approaches: C) a two-step process involving post-extrusion stretching and UV crosslinking (Reproduced with permission.[130] Copyright 2022, Wiley-VCH), and D) a one-step process optimized for high-throughput fiber production without the need for secondary alignment (Reproduced with permission.[73] Copyright 2023, Wiley-VCH). E) Schematic of electrospinning for LCE fiber fabrication, enabling the creation of complex architectures with fine structural control (Reproduced with permission.[49] Copyright 2024, AAAS).

tion, and the integration of functional fillers into complex fiber architectures.

For example, an extrusion-based method has been employed to fabricate LCE fibers by loading an LC oligomer—synthesized via an aza-Michael addition reaction—into a syringe equipped with a 17G needle.[127] The syringe was maintained at 65 °C to ensure suitable ink viscosity and pressurized to 90 psi during extrusion (**Figure 3A**). As the ink was extruded, gravity induced vertical stretching and spontaneous alignment of LC mesogens, after which the fibers were crosslinked using 365 nm UV light to

stabilize their structure and collected with a roller system. Building on this approach, coaxial spinning has been developed, where LCE shells are combined with liquid-metal cores using dual-layer nozzles to produce multifunctional fibers.[55,56] Functional fillers such as cellulose nanocrystals and CNTs have also been incorporated into LC oligomers to achieve near-infrared light-responsive LCE fibers.[113]

While melt spinning is efficient for continuous fabrication of complex, multifunctional LCE fibers, it faces challenges in controlling micrometer-scale diameters and maintaining stable material properties under strict temperature regulation.

The wet spinning method involves extruding LC oligomers through a nozzle into a coagulation bath, where solvent exchange induces rapid crosslinking of the fibers. Crosslinking can occur either in the bath or through subsequent UV irradiation. A dual-diffusion mechanism has enabled rapid fabrication of graphene/LCE composite fibers, in which the oligomers simultaneously exchange solvent and absorb catalyst, triggering in situ crosslinking without UV curing, and achieving spinning speeds of up to 4500 m h^{-1} (Figure 3B).[128] By contrast, a conventional UV-assisted strategy employs extrusion into a coagulation bath to partially crosslink the fibers, followed by mechanical stretching and UV curing under tension to align mesogens.[129] While this method yields well-ordered fibers, its multi-step processing limits the spinning speed.

While wet spinning allows rapid, continuous production of functional LCE fibers, it generally yields micrometer-scale diameters and requires specialized equipment with multi-step processing, limiting broader applicability. In dry spinning, LC oligomers are first dissolved in a solvent to form a spin-compatible ink. Upon extrusion, solvent evaporation in air induces fiber solidification, followed by orientation processes to align LC mesogens and impart anisotropy. The rheological characteristics of the spinning ink, extrusion rate, ambient temperature, and the speed of the collecting roller critically influence fiber morphology and performance.

As shown in Figure 3C, a dry-spinning setup extruded the spinning ink at 1.12 mL min^{-1}, with fibers collected by a roller rotating at 79 mm s^{-1}.[130] The fibers were stretched to twice their length during alignment and UV-crosslinked to fix mesogen orientation. Moving beyond this two-step process, a more advanced one-step dry-spinning technique was later developed through simultaneous optimization of ink formulation and equipment design (Figure 3D).[73] This method eliminates post-stretching, streamlines fabrication, and significantly enhances production efficiency and fiber performance, achieving spinning speeds of 8400 m h^{-1}, fiber diameters as small as 2.6 µm. The resulting LCE fibers exhibit a rapid actuation response of 810% s^{-1} and a driving pressure of 5.3 MPa.

Overall, dry spinning is a mature and efficient technique for fabricating LCE fibers, but it requires precise control of ink viscosity and extrusion parameters. High-performance output further depends on optimized materials and equipment to ensure consistent quality and actuator reliability.

Electrospinning is a versatile technique that employs a high-voltage electric field to draw polymer solutions into ultrafine fibers. LCE fiber structure and actuation performance are strongly influenced by ink rheology, applied voltage, and ambient conditions such as humidity and temperature. In one example, a high-voltage electric field applied between the nozzle and collection substrate enabled the fabrication of LCE fibers as fine as 4.5 µm in diameter (Figure 3E).[49] Optimizing extrusion rate, nozzle temperature, and aperture size, the LCE fibers exhibited exceptional actuation characteristics of a maximum strain of 55% and actuation stress up to 0.6 MPa. Depositing fibers along programmed trajectories further allowed the construction of 3D actuators with tailored deformation modes. In another demonstration, LCE fibers of 10 to 100 µm in diameter were fabricated without LC alignment but remained responsive to heating and near-infrared light, demonstrating large deformations and functionality in microsystems such as microrobots, microtweezers, and microfluidic pumps.[75]

Electrospinning provides scalable access to submicron LCE fibers with enhanced strain and actuation speed, though its high equipment cost and processing complexity may limit broader industrial application.

3.3. Molding Method

The molding method is a widely adopted strategy for fabricating LCE films and fibers, owing to its operational simplicity and versatility. Typically, pre-synthesized LCE oligomers are injected or deposited into a mold, where crosslinking fixes the geometry. Post-processing, often through mechanical stretching, induces mesogen alignment and imparts anisotropic actuation. The fidelity and performance of molded LCEs are governed by the oligomer's rheology, crosslinking conditions, and demolding process, which together determine mold filling, curing efficiency, and structural integrity.

As shown in **Figure** 4A, one approach injected LCE oligomers into a polytetrafluoroethylene (PTFE) tube; after crosslinking, the fiber was demolded, twisted, and stretched to generate helical mesogen alignment, enabling torsional actuation.[54] Molding also supports functional integration—for example, embedding a metal heating wire in a rubber mold, followed by precursor injection, partial crosslinking, stretching, and photopolymerization produced fibers with built-in heaters for multifunctional woven actuators (Figure 4B).[71] In another case, precursors were polymerized within PTFE tubing under mechanical deformation, yielding pre-curved fibers that were later assembled into ring-like structures capable of multimodal locomotion (Figure 4C).[69]

While molding offers simplicity, low equipment cost, and compatibility with diverse materials and geometries, its limitations include low forming precision, batch-based operation, and the inability to support continuous manufacturing. These constraints present challenges for high-throughput or precision-demanding applications.

3.4. Printing Methods

Advances in additive manufacturing have enabled LCEs to overcome the geometric limitations of traditional fabrication, allowing the creation of complex macro- and microstructures with integrated multifunctional components. This greatly expands their potential in soft robotics and smart devices. Among various additive manufacturing techniques, direct ink writing (DIW) and digital light processing (DLP) are currently most widely employed

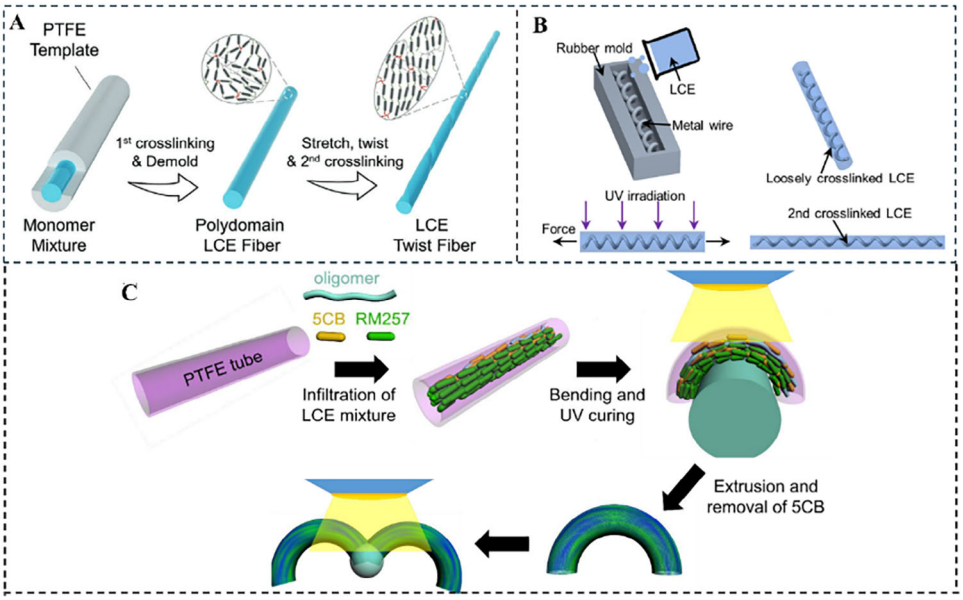

Figure 4. Fabrication of LCE fibers using the molding method. A) Schematic illustration of twisted LCE fibers fabricated by molding in a PTFE tube followed by mechanical twisting and stretching (Reproduced with permission.[54] Copyright 2022, Wiley-VCH). B) LCE fibers with integrated heating wires, prepared by embedding metal wires in the mold prior to injection and crosslinking of the LCE precursor (Reproduced with permission.[71] Copyright 2025, AAAS). C) Pre-programmed, curved LCE fibers formed via photopolymerization under mechanical deformation, subsequently assembled into ring-shaped architectures (Reproduced with permission.[69] Copyright 2023, AAAS).

for LCE fabrication. DIW, an extrusion-based method, deposits preformulated LCE inks along predefined paths, allowing real-time control of LC alignment and fabrication of 3D structures with programmable deformation. Its advantages include design flexibility, operational simplicity, and good processability, with performance depending on parameters such as extrusion pressure, nozzle diameter, printing speed, temperature, and ink rheology. DLP provides higher spatial resolution and precision, enabling finely detailed microstructures suitable for advanced applications.

The first demonstration of programming LCE molecular orientation via DIW printing was reported in 2017 (**Figure** 5A).[66] Shear-induced alignment along the print path enabled local control of LC orientation in planar and 3D structures, allowing diverse, programmable shapes. By designing regions with opposing Gaussian curvature, rapid, reversible snap-through transformations were achieved. This approach was further extended by constructing thermoresponsive 3D architectures with programmable strain magnitude and direction,[100] showing that multimaterial integration (e.g., polydimethylsiloxane (PDMS) with LCEs) and incorporation of stimuli-responsive components (magnetic, light, pH, or electric) enable multiresponsive, sophisticated structures. DIW-printed LCEs exhibited pronounced reversible contraction and high specific work output, achieving an exceptional energy density of 39 $J \cdot kg^{-1}$ and the ability to actuate loads up to 70 g.[144] This strategy provides efficient, programmable control of LC orientation, advancing soft actuators with complex shape-morphing capabilities for applications in soft robotics, artificial muscles, and biomedical devices.

In another example, locally controlled LC alignments combined with tunable isotropic–nematic transition temperatures T_{NI} encoded spatially variable thermal responses into a triangular lattice, enabling reversible, multi-state shape morphing (Figure 5B).[72]

DIW versatility extends to non-planar substrates. For example, tubular LCE-based soft pneumatic actuators (SPAs) were printed onto curved cylindrical surfaces (Figure 5C).[93] Precise path planning and mesogen alignment enabled complex multimodal actuation—including elongation, contraction, bending, and twisting—demonstrating the potential of DIW for soft robotic systems with spatially encoded mechanical responses.

To overcome the spatial limitations inherent to conventional DIW printing, which typically relies on planar layer-by-layer deposition and thus cannot produce complex 3D lattice structures, a 4D printing strategy integrates off-center continuous fiber reinforcement into the process (Figure 5D).[131] Embedded fibers act as mechanical supports, enabling freestanding 3D LCE structures. Thermal expansion mismatch between fibers and the LCE matrix produces stimuli-responsive shape transformations, from global contraction to programmable bending. Adjusting the fiber offset allows precise control of bending direction, offering highly tunable morphologies for advanced LCE actuators.

DIW is widely used for fabricating LCE actuators, enabling some 3D structures, but its layer-by-layer process and support requirements limit resolution and geometric complexity. In contrast, DLP blends LC monomers with photopolymerizable resins and solidifies them layer by layer via projected light, offering simplified processing, high spatial resolution, and strong interlayer adhesion, ideal for high-performance LCE architectures.

Photocurable thiol–acrylate LC resins have been DLP-printed into complex lattices with tunable mechanical properties across multiple length scales (Figure 5E).[143] However, molecular alignment programming and actuation were not addressed.

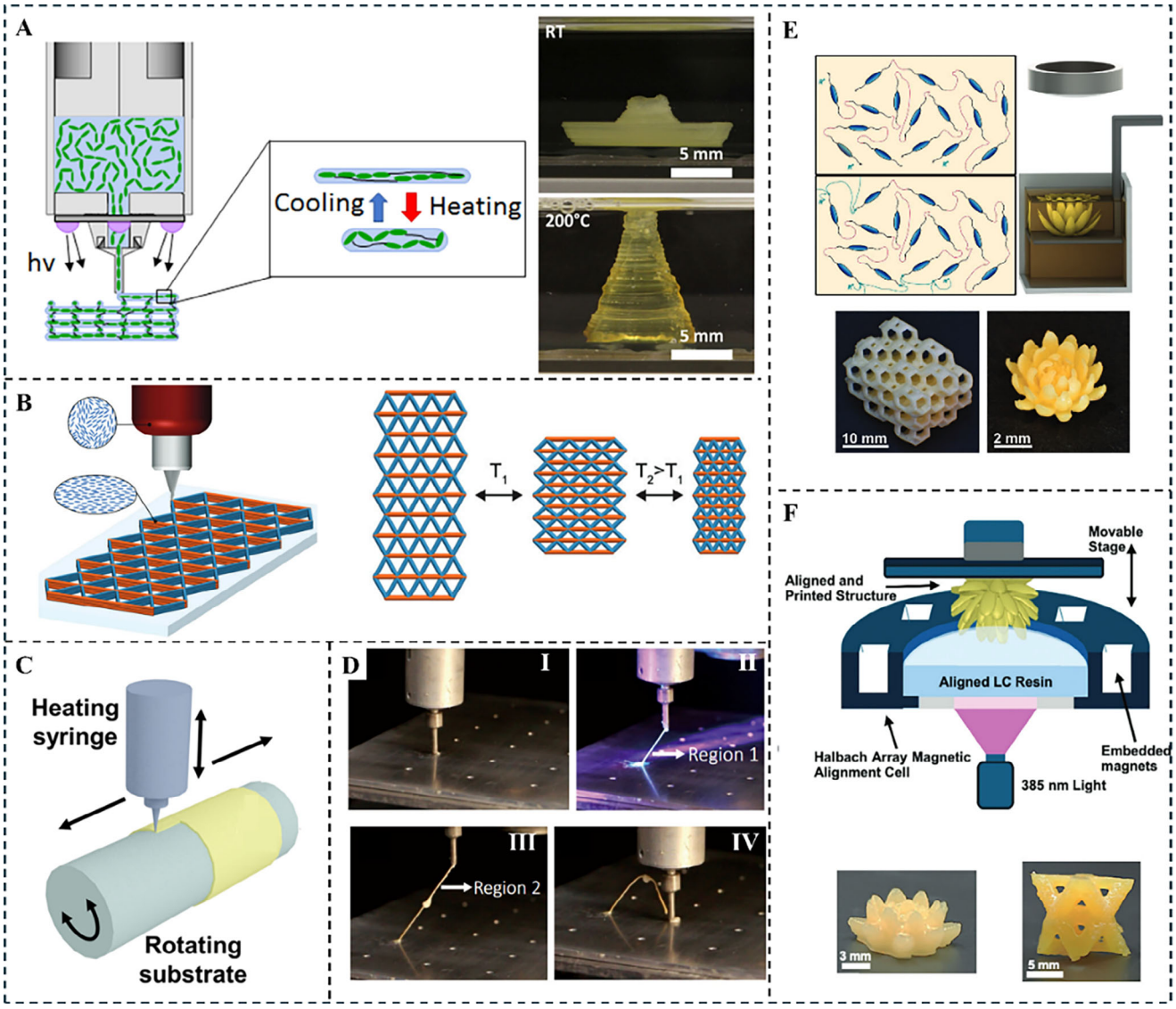

Figure 5. Fabrication of LCE Samples via printing methods. A) DIW-printed LCE structures with positive and negative Gaussian curvatures, showing asymmetric snap-through deformation upon heating, driven by mesogen reorientation in the positive-curvature regions (Reproduced with permission.[66] Copyright 2017, ACS). B) Schematic of a DIW-printed triangular lattice structure with regionally tuned T_{NI} for multistate thermally induced shape morphing (Reproduced with permission.[72] Copyright 2024, Wiley-VCH). C) LCE soft pneumatic actuators printed onto curved cylindrical surfaces via DIW, exhibiting multimodal actuation (Reproduced with permission.[93] Copyright 2023, Royal Society of Chemistry). D) Fabrication of a triangular truss unit via continuous fiber-reinforced DIW for programmable 4D shape transformation (Reproduced with permission.[131] Copyright 2023, Springer Nature). E) Schematic of DLP printing and the fabricated lattice and lotus structures, illustrating multiscale, high-resolution fabrication of complex geometries. (Reproduced with permission.[143] Copyright 2020, Wiley-VCH). F) 3D structures with directional alignment, including lotus and lattice motifs, fabricated using DLP-based photopolymerization printing (Reproduced with permission.[67] Copyright 2024, Wiley-VCH).

To program mesogen orientation, external fields such as a 100 mT magnetic field have been applied during printing to align the mesogens in main-chain LCEs, producing intricate 3D structures with enhanced anisotropy (Figure 5F).[67] Shear-induced alignment combined with embedded optical sensors enables thermally responsive, multifunctional LCEs capable of actuation and environmental sensing.[132] These advances highlight DLP-printed LCEs as multifunctional intelligent materials integrating actuation and sensing within a single platform.

4. Practical Applications of LCE Actuators

Recent advances in LCE processing and fabrication have enhanced structural programmability and multifunctionality, accelerating their integration into next-generation intelligent systems. Owing to tunable actuation and programmable anisotropic architectures, LCE-based actuators have advanced rapidly over the past decade, as illustrated in **Figure 6**.

In 1980, Finkelmann and colleagues successfully synthesized LCEs and developed a two-step crosslinking strategy

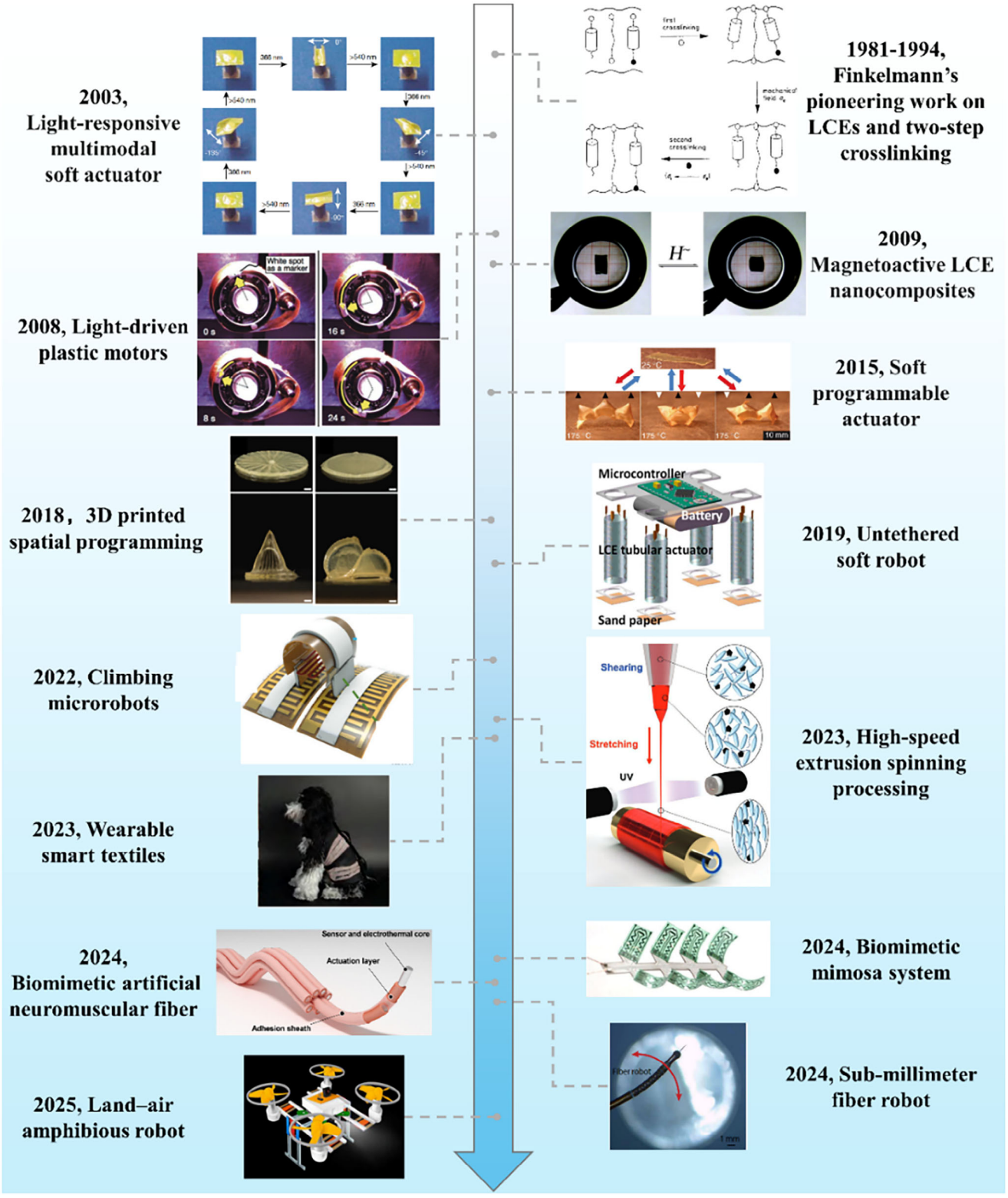

to produce monodomain LCEs with controllable preparation, enabling predictable and reversible shape transformations and laying a key experimental foundation for achieving large, controllable strains.[145,146] Later, azobenzene photoisomers were incorporated into the LCE network, allowing high-precision light-induced bending of films under polarized light. This approach not only established a new route for light-driven actuation but also significantly broadened the stimuli-responsiveness of LCEs, paving the way for light-controlled soft robotics.[147]

Previously reported LCEs primarily exhibit contraction, expansion, and bending, making the expansion of deformation modes crucial for practical applications. To address this, a laminated film was fabricated by integrating an azobenzene-containing LCE layer with a flexible polyethylene sheet, yielding a composite that combines high photoresponsivity with robust mechanical properties. Building on this design, the laminated film was incorporated with axles and pulleys to construct a light-driven motor capable of directly converting light energy into mechanical work and executing complex rotational motions.[148]

To further enhance multimodal stimuli-responsiveness, functional nanofillers such as superparamagnetic nanoparticles[149] and CNTs[150] have been embedded into LCE matrices, producing multifunctional nanocomposites with tunable actuation performance. For example, superparamagnetic nanoparticles enable rapid localized heating under external magnetic fields to trigger elastomer actuation, while poly(p-phenyleneethynylene) (PPE)-functionalized single-walled CNTs (PPE-SWCNTs) leverage strong visible and near-infrared absorption to facilitate efficient actuation under infrared irradiation.

The programmable modulation of shape endows actuators with versatile functionalities and broadens their application scope. The advent of photoalignment techniques enabled precise molecular orientation control, achieving microscale shape reconfiguration with high fidelity.[135] These advances established the fundamental platform for predictable and repeatable actuation, positioning LCEs as intelligent, responsive materials.

The integration of 3D printing technologies subsequently revolutionized LCE fabrication by introducing unprecedented design flexibility and spatial control.[144] Digital manufacturing approaches allowed for the rapid prototyping of complex geometries and orientation-specific architectures, facilitating the programmable construction of LCE-based actuators with tailored deformation profiles. These capabilities greatly enhanced both fabrication efficiency and functional performance, laying the groundwork for widespread adoption in multifunctional systems.

Empowered by these innovations, LCE actuators have been successfully incorporated into diverse application domains—including multimodal robotics, artificial muscles, smart textiles, self-sensing systems, and medical microrobotics. For instance, the integration of pre-patterned heating circuits, microcontrollers, and energy storage components within LCE matrices has led to the development of wireless soft robots capable of multimodal locomotion.[65] In another example, the incorporation of electroadhesive interfaces significantly enhanced robotic mobility, enabling effective traversal across varied surface topographies such as undulating, inclined, and curved terrains.[151]

Meanwhile, the development of high-throughput spinning technologies has extended LCE applications into fiber-based systems. Inspired by spider silk, ultrafast fiber extrusion strategies have been established to produce high-performance LCE fibers.[73] These approaches have led to the emergence of LCE-based intelligent textiles, offering promising opportunities for future personalized smart clothing systems.[76]

In the realm of self-sensing actuation, the inherent softness and responsiveness of LCEs make them ideal candidates for bioinspired devices. Recent breakthroughs include mimosa-like responsive systems[77] and artificial neuromuscular fibers[152] that integrate sensing and actuation in a single material platform—offering promising routes toward tactile perception systems and neuromorphic actuation networks.

LCEs also exhibit strong compatibility with micro-/nanofabrication techniques, enabling the development of soft, miniature continuum robots for precision medical applications. A notable example is a sub-millimeter LCE-based microrobot, exhibiting decoupled macroscopic and microscopic motion capabilities.[5] This design allows for targeted navigation within complex biological environments, offering a novel solution for minimally invasive surgical operations.

System-level integration has propelled LCE actuators toward multifunctional intelligent platforms. A recent study demonstrated a land–air amphibious microrobot that synergistically combined LCE actuators, shape memory polymers, and rigid electronics, demonstrating multimodal locomotion and adaptive task capabilities.[153] Looking ahead, the convergence of LCE actuators with flexible electronics, microscale energy storage, and multimodal sensing could enable autonomous water–land–air robots capable of environment-aware decision-making and intelligent response.

To provide a comprehensive overview of emerging trends, this section outlines the evolution and application of LCE actuators across five domains: robotics, artificial muscles, smart textiles, self-sensing systems, and medical devices. Collectively, these

Figure 6. Developmental trajectory of LCE actuators. Key advancements include: pioneering work on LCEs and two-step crosslinking (Reproduced with permission.[145] Copyright 1994, Wiley-VCH); light-responsive multimodal soft actuator (Reproduced with permission.[147] Copyright 2003, Springer Nature); light-driven plastic motors (Reproduced with permission.[148] Copyright 2008, Wiley-VCH); magnetoactive LCE nanocomposites (Reproduced with permission.[149] Copyright 2009, Royal Society of Chemistry (RSC)); soft programmable actuator (Reproduced with permission.[135] Copyright 2015, AAAS); 3D printed spatial programming (Reproduced with permission.[144] Copyright 2018, Wiley-VCH); untethered soft robot (Reproduced with permission.[65] Copyright 2019, AAAS); climbing microrobots (Reproduced with permission.[151] Copyright 2022, Proceedings of the National Academy of Sciences of the United States of America (PNAS)); high-speed extrusion spinning processing (Reproduced with permission.[73] Copyright 2023, Wiley-VCH); wearable smart textiles (Reproduced with permission.[76] Copyright 2023, ACM); biomimetic mimosa system (Reproduced with permission.[77] Copyright 2024, Springer Nature); biomimetic artificial neuromuscular fiber (Reproduced with permission.[152] Copyright 2024, Elsevier); Sub-millimeter fiber robot (Reproduced with permission.[5] Copyright 2024, AAAS); land–air amphibious robot (Reproduced with permission.[153] Copyright 2025, Springer Nature).

advances highlight the transformative potential of LCEs as intelligent materials for next-generation multifunctional technologies. Nevertheless, several key challenges must be addressed before widespread deployment. First, further improvements in actuation speed, durability, and power density are needed to meet performance demands in complex environments. Second, achieving seamless integration of sensing, response, and multimodal actuation within a single platform remains elusive; bioinspired structural designs coupled with AI-driven control may enable closed-loop intelligent systems. Third, progress in scalable, low-cost, and precisely controllable fabrication is critical to translating laboratory advances into practical, large-scale applications.

4.1. Robotics

4.1.1. Soft Robots

Soft robots, built from compliant and stimuli-responsive materials, offer superior adaptability, safety, and environmental interaction compared to rigid robotic systems. Among available actuator materials, LCEs stand out for their mechanical flexibility, facile processability, and responsiveness to multiple stimuli, including heat, light, and electromagnetic fields.[65,154–156] Advances in formulations and fabrication now allow LCE actuators to achieve precise, programmable deformations with high degrees of freedom, making them especially suited for soft robotics in unstructured or dynamic environments. Applications span search and rescue, environmental monitoring, and biomedical devices.

Recent work has demonstrated LCE-based robots with multimodal locomotion and environmental adaptability. For instance, a compact actuator with programmable anisotropic strain was integrated into a deformable body with an electroadhesive layer, yielding a soft robot capable of climbing, attaching, and detaching across diverse surfaces—from pipe interiors to curved or undulating geometries (**Figure 7A**).[151] In another example, a ring-shaped LCE actuator achieved continuous self-rotation under constant light or heat, enabling sustained locomotion across glass tubes, solid surfaces, and liquid media (Figure 7B).[157] These demonstrations highlight the versatility and robustness of LCE-driven systems in enabling autonomous navigation and adaptive motion across challenging environments.

By integrating distributed heating circuits within LCE structures, localized thermal actuation can be achieved, enabling independent regional responses and thus complex, programmable deformations for multimodal robotic motion. A caterpillar-inspired soft robot exemplified this strategy: a thin-film LCE actuator combined with a silver nanowire heating circuit produced bidirectional crawling by selectively activating specific regions, allowing navigation even through narrow tunnels (Figure 7C).[74] Similarly, embedding heating wires in a tubular LCE actuator, coupled with an electronic control system, enabled precise electrical manipulation of multimodal deformations. Incorporation of a microcontroller and onboard power supply further yielded an untethered, wireless soft robot with stable, remotely controlled locomotion (Figure 7D).[65] Together, these advances underscore the potential of thermally programmed LCEs for agile, autonomous soft robotics.

Beyond crawling and walking, jumping provides soft robots with key advantages in obstacle traversal, gap bridging, and high-speed locomotion. A light-driven LCE robot (**Figure 8A**) exemplifies this mode: photoisomerization of azobenzene molecules induces rapid contraction and bistable deformation, enabling efficient energy storage and release. The robot achieves a remarkable jump height up to 15.5 times its body length and a launch speed of 880 body length per second, underscoring the potential of photoresponsive LCEs for agile motion.[122]

Self-rolling, another prevalent locomotion strategy, leverages geometric or structural asymmetry to achieve directional mobility. Thermally actuated LCE fibers with asymmetric ends combined helical and torsional deformations to produce autonomous rolling and adaptive steering in response to environmental boundaries (Figure 8B),[158] suitable for navigation in confined spaces such as mazes. DIW-fabricated LCE tiles with programmable hinge joints enabled sequential folding via materials with distinct transition temperatures, yielding self-rolling polyhedral robots with tunable locomotion (Figure 8C).[120] A tensegrity-inspired design integrating LCE tendons, elastic cords, and rigid frames further demonstrated programmable trajectories and adaptive path-following (Figure 8D).[159] Collectively, these examples highlight rolling as a versatile and scalable approach for LCE-based robotic navigation.

4.1.2. Amphibious Robots

While soft robots have demonstrated multimodal locomotion and task adaptability, a key barrier to real-world deployment lies in seamless transitions across heterogeneous environments. Critical missions such as search and rescue, environmental monitoring, and medical intervention often demand efficient traversal between land, water, and even aerial domains.[160] Conventional robotic systems typically experience sharp declines in performance or outright failure when facing such shifts due to the contrasting physical properties of these media. Addressing this challenge requires soft robots that integrate mechanical compliance with real-time reconfigurability and adaptive responsiveness, enabling robust cross-environment locomotion in unstructured and dynamic settings.

Representative advances illustrate the potential of LCE-based systems for cross-environment adaptability. One study demonstrated an LCE actuator integrated with shape memory polymers for continuous morphological transformation and reversible shape locking, enabling a 25 g land–air microrobot capable of transitioning between terrestrial locomotion and aerial flight by adjusting its propeller–ground angle (**Figure 9A**).[153] The robot reached an impressive terrestrial speed of 18.20 body lengths per second, showcasing high adaptability through lightweight, reconfigurable design.

In another approach, a tetherless amphibious soft robot was constructed from an LCE–liquid metal multilayer ribbon and actuated by high-frequency alternating magnetic fields (Figure 9B).[121] Inductive heating allowed multimodal locomotion, including terrestrial crawling, flipping, and swimming, with directional control achieved via directional Lorentz forces. These designs highlight the promise of LCE-based platforms for intelligent, multimodal operation across land, water, and air.

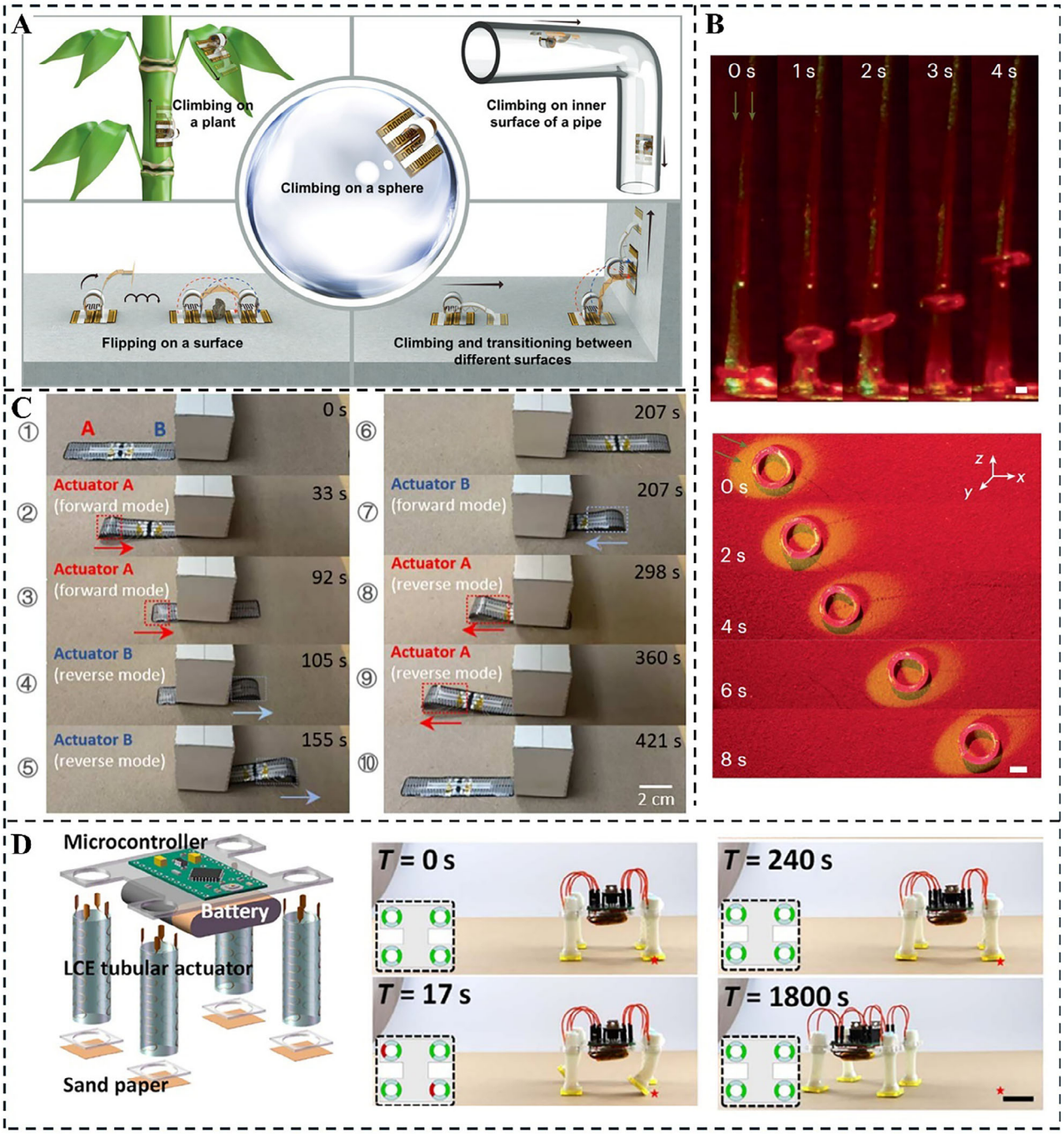

Figure 7. Applications of LCE actuators in robotics. A) Schematic of a soft microrobot climbing across various complex surfaces including spheres, plants, and pipelines (Reproduced with permission.[151] Copyright 2022, PNAS). B) Motion snapshots of an LCE ring rolling on flat and tapered glass pipettes (Reproduced with permission.[157] Copyright 2024, Springer Nature). C) Locomotion sequence of a caterpillar-inspired soft crawling robot navigating a narrow tunnel (Reproduced with permission.[74] Copyright 2023, AAAS). D) Configuration of an untethered soft robot (comprising a microcontroller, battery, and four LCE tubular actuators) with corresponding walking displacement data (black curve) (Reproduced with permission.[65] Copyright 2019, AAAS).

4.2. Artificial Muscles

LCE fibers share structural and functional similarities with biological muscles, positioning them as promising building blocks for artificial muscle systems. These soft actuators reproduce the contraction–extension behavior of natural tissue by responding to diverse stimuli, including heat, light, electric and magnetic fields, and pneumatic pressure.[161–163] Recent advances in LCE synthesis and processing have substantially improved actuation speed, force output, and contraction ratios, expanding their

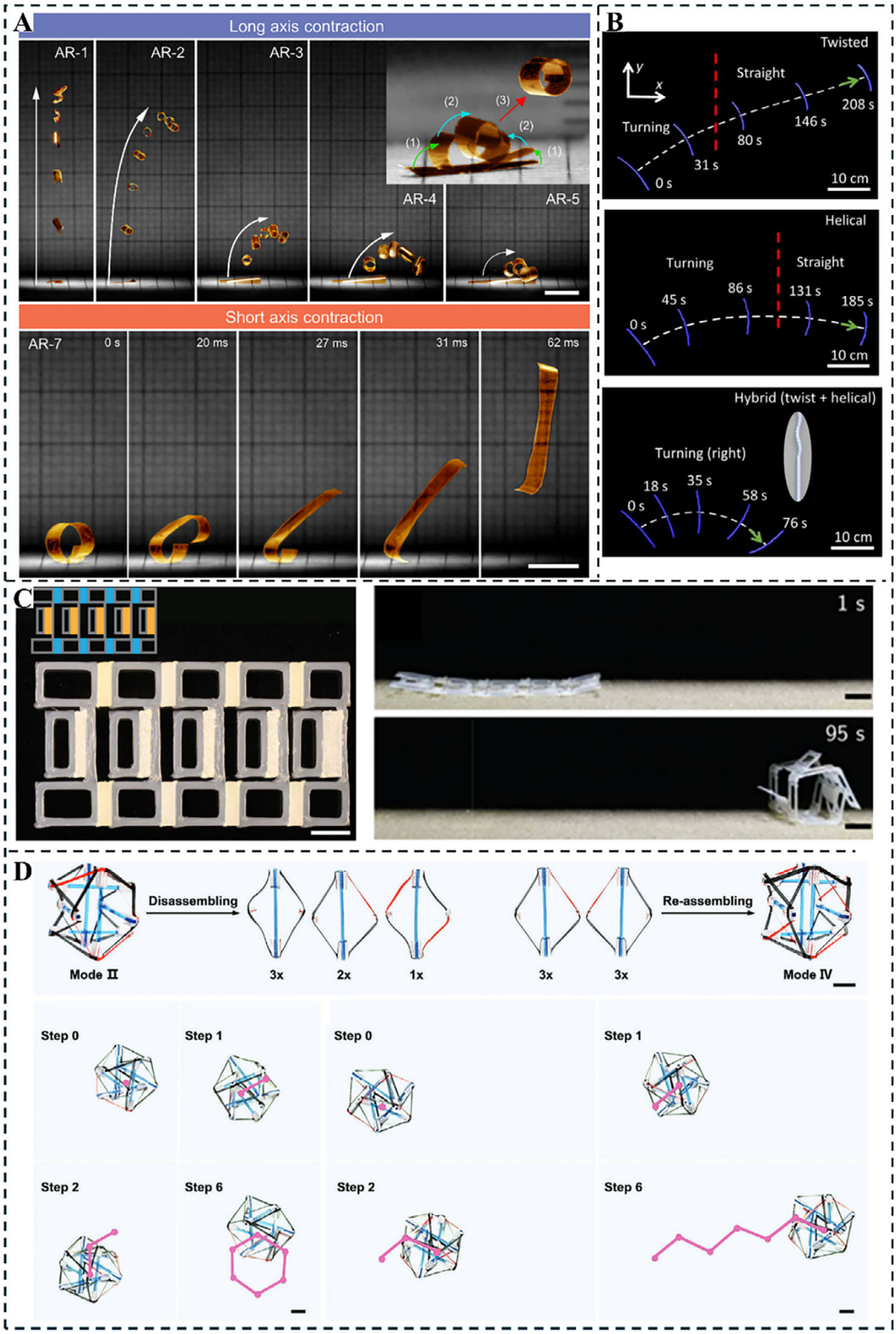

Figure 8. Applications of LCE actuators in robotics. A) Light-induced contraction of LCP films enabling impacting, coiling–jumping, and kicking–jumping motions along different axes (Reproduced with permission.[122] Copyright 2021, Elsevier). B) Motion trajectories of thermally responsive twisted and helical LCE-based self-rolling robots (Reproduced with permission.[158] Copyright 2023, AAAS). C) Structure and self-propulsion sequence of a self-rolling robot composed of LCEs with different T_{NI} values and polymer tiles (blue: low-T_{NI} LCE, orange: high-T_{NI} LCE, gray: polymer tiles) (Reproduced with permission.[120] Copyright 2019, AAAS). D) Motion trajectory diagram of a hybrid tensegrity-inspired self-rolling robot actuated by thermally responsive cables under different configurations (Reproduced with permission.[159] Copyright 2024, Wiley-VCH).

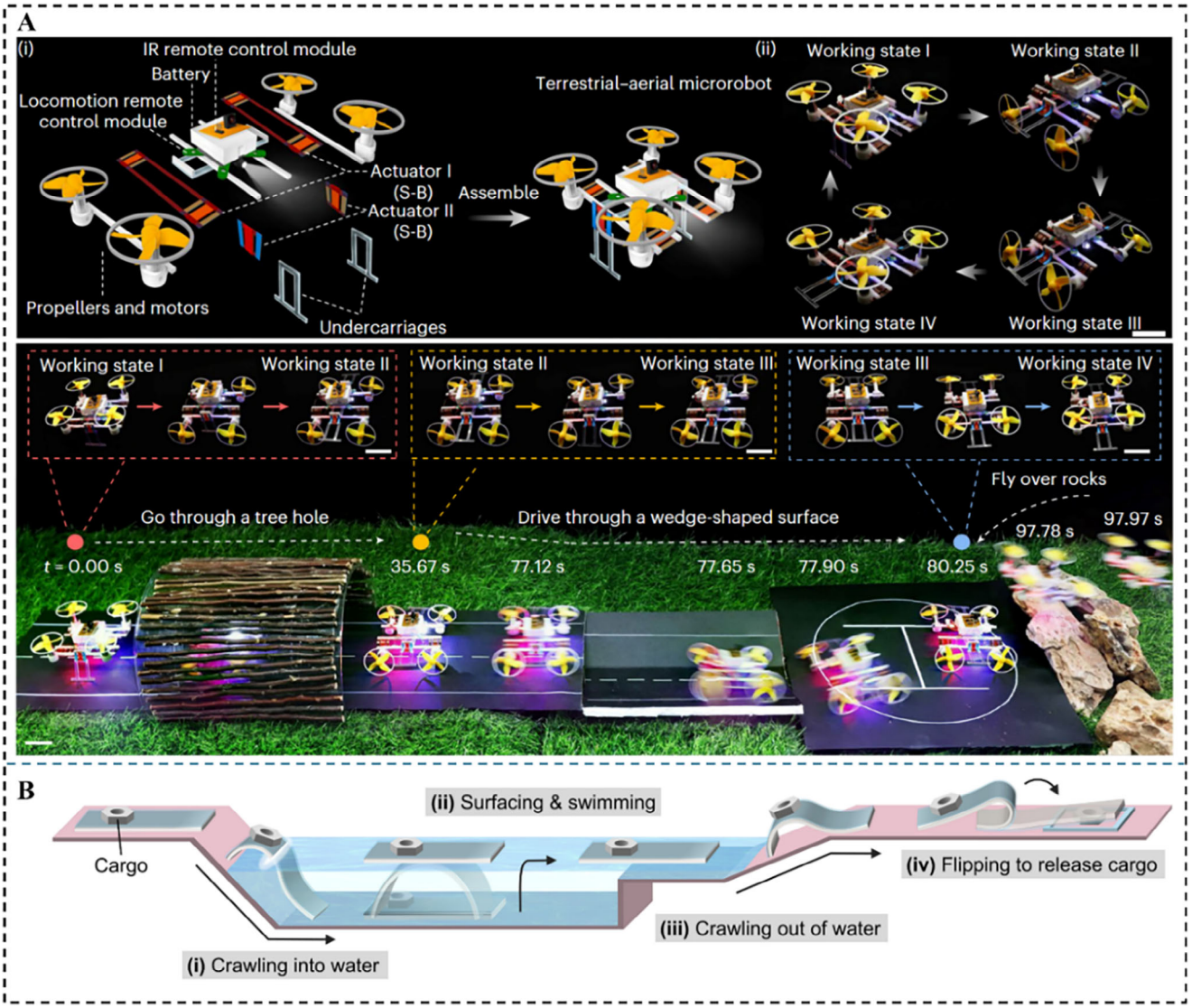

Figure 9. Applications of LCE actuators in robotics. A) Schematic of a land–air amphibious microrobot and its operation in representative complex environments, including tree hole navigation, locomotion on an inclined wedge, and aerial traversal over rocky terrain (Reproduced with permission.[153] Copyright 2025, Springer Nature). B) Schematic of multimodal amphibious soft robot performing locomotion and cargo transport in both terrestrial and aquatic environments (Reproduced with permission.[121] Copyright 2025, Elsevier).]

potential for soft robotics and biomedical applications. This section reviews recent developments in the design, optimization, and application of LCE-based artificial muscles, highlighting their performance enhancement and integration into functional systems.

To enhance the photothermal responsiveness of LCE fibers, carbon-based materials are often incorporated to improve light absorption and thermal conversion efficiency. For instance, dry-spun continuous LCE fibers coated with polydopamine (PDA)-modified MXene ink demonstrated exceptional load-bearing capability, lifting weights up to 1000 times their own mass (**Figure 10A**), thereby highlighting their potential for high-performance actuation.[114] Similarly, bioinspired dry-spun microfibers with precise molecular alignment exhibited superior actuation speed, force generation, and durability, and were successfully integrated into skeletal mimicry systems, offering strong potential for intelligent soft actuators (Figure 10B).[73] In another approach, electrospun LCE microfibers coated with PDA enabled near-infrared (NIR) remote actuation (Figure 10C).[75] When coupled with a 3D-printed robotic arm, these actuators achieved controlled bending and object manipulation, underscoring their promise for smart robotics, micro-manipulation, and flexible electronics.

Although applications of LCE artificial muscles in deep-sea environments remain limited, structural design strategies have demonstrated their feasibility under extreme conditions. For example, knot-configured LCE fibers with embedded heating wires maintained robust contraction performance at 30 MPa, with the square knot design, in comparison with triple knot, twist knot, exhibiting the fastest response (Figure 10D).[164]

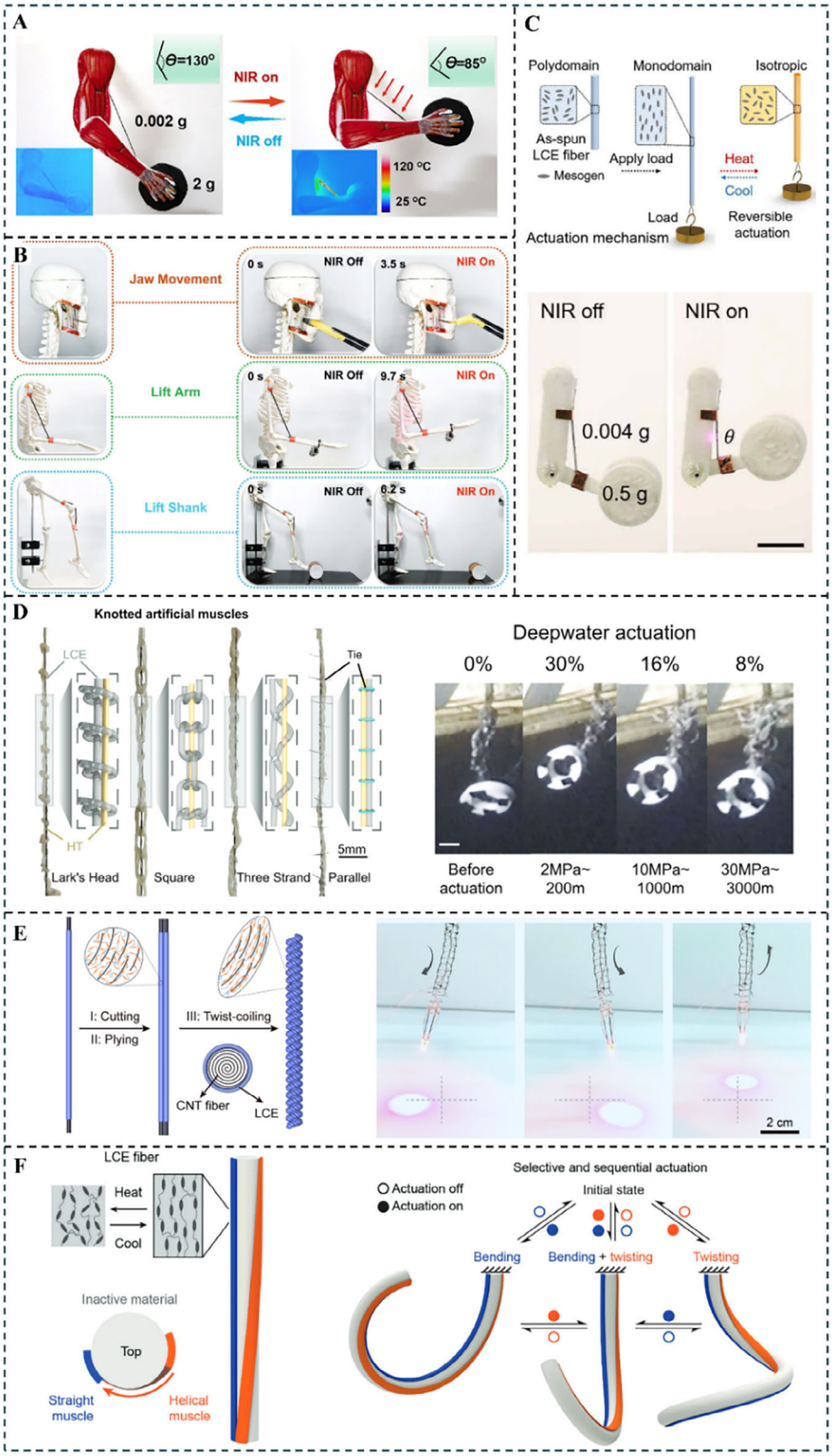

Figure 10. Applications of LCE actuators in artificial muscles. A) Bending and recovery of a robotic arm driven by NIR-responsive LCE fiber actuators (Reproduced with permission.[114] Copyright 2023, RSC). B) Bioinspired muscle contraction mimicking skeletal systems using NIR-activated LCE fibers (Reproduced with permission.[73] Copyright 2023, Wiley-VCH). C) Actuation mechanism of near-infrared-responsive LCE fibers showing phase transition-induced contraction (Reproduced with permission.[75] Copyright 2021, AAAS). D) Actuation of LCE fiber actuators under varying hydrostatic pressures with different knotting configurations (Reproduced with permission.[164] Copyright 2024, Wiley-VCH). E) Preparation of LCE/CNT composite fibers for endoscope robot motion, driven by spiral-shaped actuators (Reproduced with permission.[165] Copyright 2023, ACS). F) Multimodal deformation of a soft arm through selective activation of LCE fibers for object manipulation (Reproduced with permission.[166] Copyright 2024, Wiley-VCH).

Beyond extreme environments, LCE-based artificial muscles are increasingly advancing toward biomedical applications. A representative example is a self-healing CNT–LCE helical composite fiber with high contraction ratio, rapid response, and durability, which enabled a multi-degree-of-freedom endoscopic system for minimally invasive surgery (Figure 10E).[165] Similarly, inspired by the structure of an elephant's trunk, a biomimetic soft robotic arm was developed by integrating LCE muscle fibers onto a passive, flexible cylindrical body in both linear and helical configurations (Figure 10F).[166] In both cases, selective activation of LCE muscles in different orientations allowed programmable, multidirectional deformation–enabling flexible endoscopic navigation in the former and adaptive bending–twisting morphing in the latter–thereby underscoring the potential of LCE muscles in medical and bioinspired robotic systems.

4.3. Smart Textiles

LCE fibers fabricated via spinning techniques combine high mechanical performance with tunable morphology, precise dimensional control, and scalability. These attributes make them excellent candidates for functional yarns that can be processed using conventional textile techniques to create multifunctional, structurally complex smart textiles.[76,167] Such textiles can actively respond to environmental or physiological stimuli, offering promising applications in motion assistance, wearable rehabilitation, and personal thermal regulation.

A key challenge in smart textile development is integrating textile engineering strategies to achieve programmable 3D deformation and tailored functional responsiveness. Knitted architectures have been used to enhance deformability and modularity, allowing LCE fibers to be reversibly assembled and reconfigured between patterns such as "rib–plain–rib" and "plain–rib–plain" (**Figure 11**A).[127] When patterned along predefined pathways, these textiles exhibit diverse 3D behaviors—including folding, twisting, and bending. A representative demonstration involves a four-petal LCE flower that dynamically closes under electrical stimulation.

Hybrid weaving strategies, which integrate LCE fibers with conventional yarns, offer another route to programmable 3D deformation. By combining soft and stiff LCE fibers, diverse textile patterns—plain, satin, weft rib, and twill—were created, with the twill structure, woven from stiff LCE fibers, achieving the highest blocking force (1–2 N cm^{-1}) and the weft rib structure exceeding 10% reversible strain (Figure 11B).[168] Radially patterned fabrics combining stiff LCE fibers with rigid yarns transformed from flat discs into conical shapes under thermal stimulation, while LCE fibers with unimodal or bimodal actuation were integrated into cotton fabrics to create predefined functional patterns that enabled localized wrinkling (Figure 11C).[129] These approaches demonstrate the capability of LCE-based textiles for programmable, morphing, and thermoresponsive applications.

LCE fibers produced via conventional spinning typically align molecules along the fiber axis under shear, resulting in thermally induced contraction upon stimulation. Achieving molecular orientations orthogonal to the fiber axis–and thus thermally induced elongation–has long been a central challenge. A recent study showed that by controlling the mesophase during extrusion (smectic vs nematic), LCE molecules can be aligned either perpendicular or parallel to the fiber axis, yielding reversible elongation of ≈30% and contraction of ≈49%, respectively (Figure 11D).[14] Integrating both fiber types into textiles enabled spatially distinct actuation, creating opportunities for intelligent textile actuators.

With the rapid advancement of flexible intelligent materials, wearable devices are shifting from rigid designs toward flexible, multifunctional platforms. Owing to their responsiveness to diverse stimuli (electric, magnetic, thermal, optical, pneumatic) and their ability to undergo large, reversible deformations, LCEs represent a promising material for wearable technologies. LCE-based fibers combine comfort and compliance with dynamic adaptability, making them well suited for smart garments and motion-assistive systems.

One approach involved integrating LCE fibers into textiles using garter stitch techniques, where flat-lying loops facilitated thermally induced shrinkage and localized protrusion in both cylindrical and planar knitted fabrics (Figure 11E).[39] Further weaving of LCE fibers with conventional cotton yarns produced a smart shirt with temperature-responsive behavior. As the body or ambient temperature rises, the LCE fibers contract, actuating microscale structures that open "pores" in the fabric, thereby facilitating intelligent thermal regulation. Expanding this concept, another strategy combined textile manufacturing with embedded heating elements and conductive coatings to produce multifunctional, machine-washable LCE-based fabrics (Figure 11F).[76] Demonstrated applications included an adaptive sports bra, foldable lighting, shape-shifting curtains, and a compression jacket for animal care. Together, these advances highlight the promise of LCE fibers for next-generation smart textiles, where functionality, comfort, and adaptability converge in applications ranging from intelligent clothing to responsive architecture and personalized healthcare.

4.4. Self-Sensing Devices

While LCEs exhibit energy output and linear contraction comparable to or exceeding natural muscle fibers, they inherently lack sensory and signal-processing capabilities.[169–172] Conventional LCE actuators therefore cannot autonomously perceive external stimuli or their own deformation. Current research focuses on integrating sensing, actuation, and signal processing into multifunctional LCE systems, enabling real-time monitoring, environmental awareness, and adaptive responsiveness. Such bioinspired self-sensing LCE actuators show strong potential for applications in wearable devices, human–machine interfaces, and soft robotics.

The first demonstrations of LCE-based self-sensing devices emerged in 2021 (**Figure 12**A).[56] A core-shell 3D printing method produced iLCE fibers with an LCE shell and liquid metal core, achieving cyclic, programmable actuation from 1D fibers to complex 2D and 3D architectures. The conductive core endowed the fibers with intrinsic sensing and closed-loop control, broadening their applicability in wearable devices and intelligent soft robotics. In another example, inspired by Mimosa pudica, an information-interaction system integrating sensing, actuation, and signal processing was reported.[77] This design introduced a

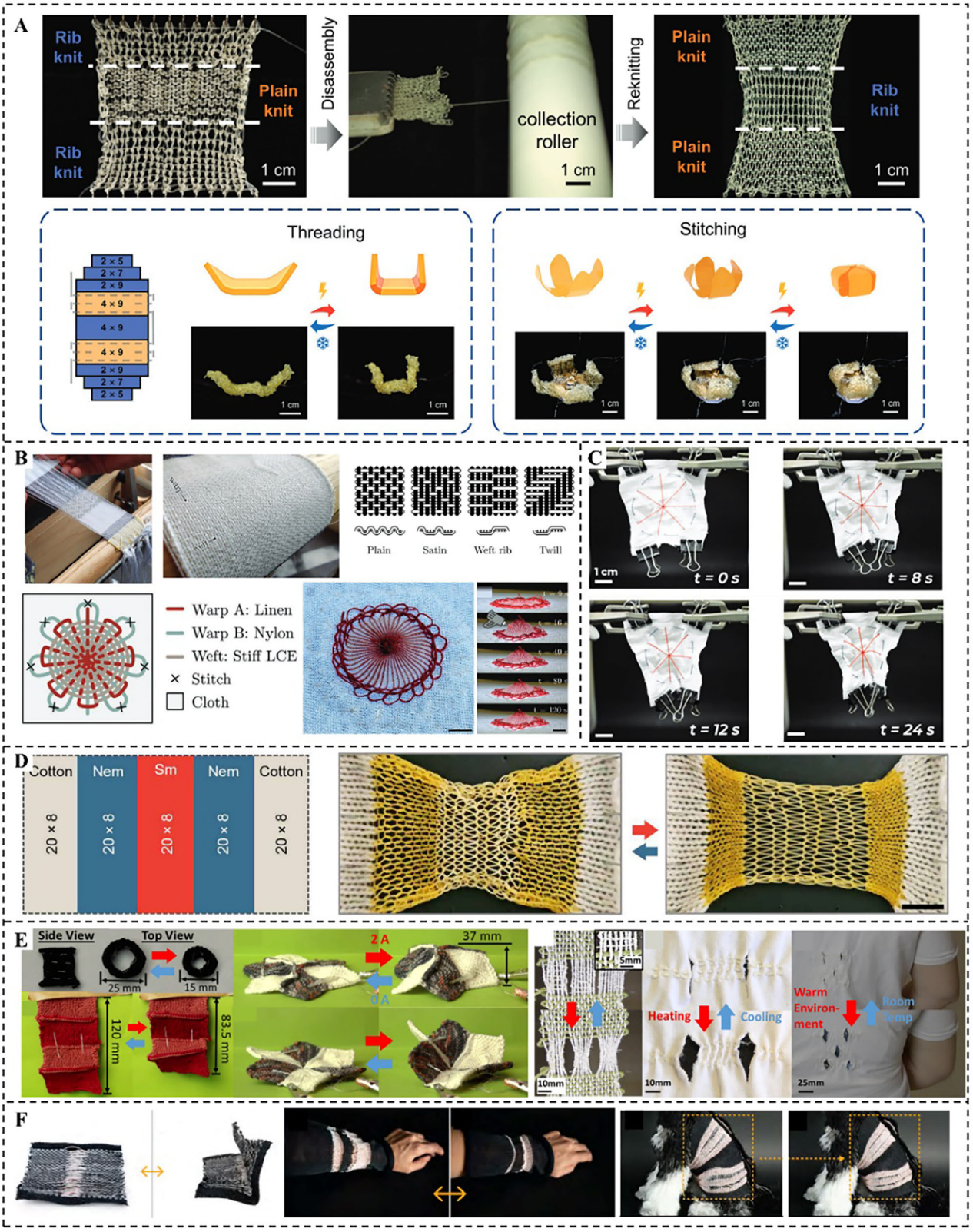

self-propelled gate (SPG)—a liquid crystal oligomer-based logic switch—capable of cascaded signal transmission. A biomimetic mimosa system constructed from eight interconnected SPGs reproduced the cascading leaf-folding behavior of the natural plant (Figure 12B). These advances underscore the potential of LCEs for building multifunctional, stimulus-responsive platforms with integrated perception and actuation.

Neuromuscular fiber-like structures have been fabricated using rotational molding techniques, embedding a highly conductive liquid metal core within an LCE shell.[152] This hybrid design combines the high conductivity of the liquid metal with the reversible deformation of the LCE, resulting in multifunctional smart fiber units capable of sensing, self-diagnosis, and actuation. When assembled into bundles, the fibers emulate biological neuromuscular pathways and enable reflex-like behavior. In a proof-of-concept artificial knee-jerk model, external mechanical stimulation was rapidly detected and converted into contraction, producing a swift forward swing of an artificial leg (Figure 12C). This demonstration highlights the potential of LCE-based systems to unify sensing and actuation for biomimetic feedback devices.

4.5. Medical Devices

LCEs, as stimuli-responsive materials combining the orientational order of liquid crystals with the elasticity of polymer networks, are gaining increasing attention in medical device applications. Their programmable anisotropic deformation, rapid responsiveness, and favorable biocompatibility make them well suited for flexible, minimally invasive, and multifunctional devices. These attributes have been exploited in diverse biomedical contexts, including microsurgical robotics, adaptive wound dressings, and implantable therapeutic systems. By enhancing adaptability, conformability, and intelligent responsiveness, LCEs offer a versatile material platform for personalized healthcare, positioning LCE-based medical devices as a key frontier in next-generation smart biomedical technologies.

A recent study demonstrated an LCE-based metamaterial with optimized biaxial actuation and reduced activation temperature, which, when integrated into medical dressings, enabled rapid hemostasis and accelerated tissue regeneration on complex wounds (**Figure 13A**).[6] Compared to conventional medical dressings, this approach offers superior conformability and stimulus-responsiveness, highlighting the potential of LCEs in developing intelligent therapeutic materials.

At the device scale, a sub-millimeter continuum fiber robot incorporating photoresponsive LCE segments and ultrathin optical fibers achieved coordinated macro–micro control for minimally invasive interventions (Figure 13B).[5] Gross navigation was provided by mechanical actuation, while localized micromotion was enabled by light-triggered deformation, addressing the challenge of combining large-range mobility with high-precision manipulation in intracavitary therapy.

Extending to implantable applications, a photothermally actuated LCE-carbon black cuff with tunable tension was demonstrated for stress urinary incontinence (SUI) and evaluated in a urinary tract model under infrared illumination (Figure 13C).[173] Implanted around the bladder neck of multiparous female rabbits, the cuff maintained continence while allowing controlled voiding, highlighting its potential as a dynamic, minimally invasive therapeutic device for SUI.

5. Conclusion and Outlook

This review has summarized recent advances in LCE actuators, spanning material design, actuation mechanisms, fabrication methods, and device architectures, and highlighted their broad applications in robotics, artificial muscles, smart textiles, self-sensing systems, and medical devices. While remarkable progress has been achieved, several challenges remain, particularly in optimizing actuation performance, integrating multifunctional intelligence, and scaling up manufacturing. Future research will likely focus on material innovations that enhance speed, durability, and power density, as well as system-level strategies that couple actuation with sensing, energy storage, and control. By addressing these challenges through interdisciplinary approaches, LCE actuators are poised to deliver higher performance, expanded functionality, and adaptive intelligence, paving the way toward their widespread adoption in next-generation smart technologies.

5.1. Performance Optimization

5.1.1. Power Density

LCE actuators can reach power densities comparable to biological muscles, but their softness limits driving force and mechanical strength under high-load or high-speed conditions. Approaches such as increasing crosslinking density, incorporating nanofillers, or using crystallizable LCEs enhance force but often reduce actuation strain and slow response, reflecting a

Figure 11. Applications of LCE actuators in smart textiles. A) Knitted LCE smart textile initially constructed in a "rib–plain–rib" pattern and later reconfigured into a "plain–rib–plain" pattern, demonstrating reversibility and reusability. A 4-petal LCE flower design exhibits dynamic opening and closing under electrical stimulation (Reproduced with permission.[127] Copyright 2023, Wiley-VCH). B) Loom-woven textile patterns (plain, satin, weft rib, and twill) fabricated from soft and stiff LCE fibers, and thermal actuation of a radially patterned disc transforming into a conical shape (Reproduced with permission.[168] Copyright 2023, Wiley-VCH). C) Cotton fabrics embroidered with unimodal and bimodal LCE fibers forming predefined patterns that enable controllable actuation under thermal stimuli (Reproduced with permission.[129] Copyright 2024, Wiley-VCH). D) Hybrid textiles composed of nematic and smectic LCE fibers exhibited spatially distinct thermal actuation, with pore areas decreasing in nematic regions and increasing in smectic regions upon heating. (Reproduced with permission.[14] Copyright 2025, AAAS). E) Thermally responsive actuation of tubular and flat knitted LCE textiles and thermally actuated pore opening in a cotton shirt embedded with LCE fibers (Reproduced with permission.[39] Copyright 2019, ACS). F) Woven LCE-fiber-based smart textiles with integrated heating elements used in compressive fabrics and a dog compression jacket (Reproduced with permission.[76] Copyright 2023, ACM).

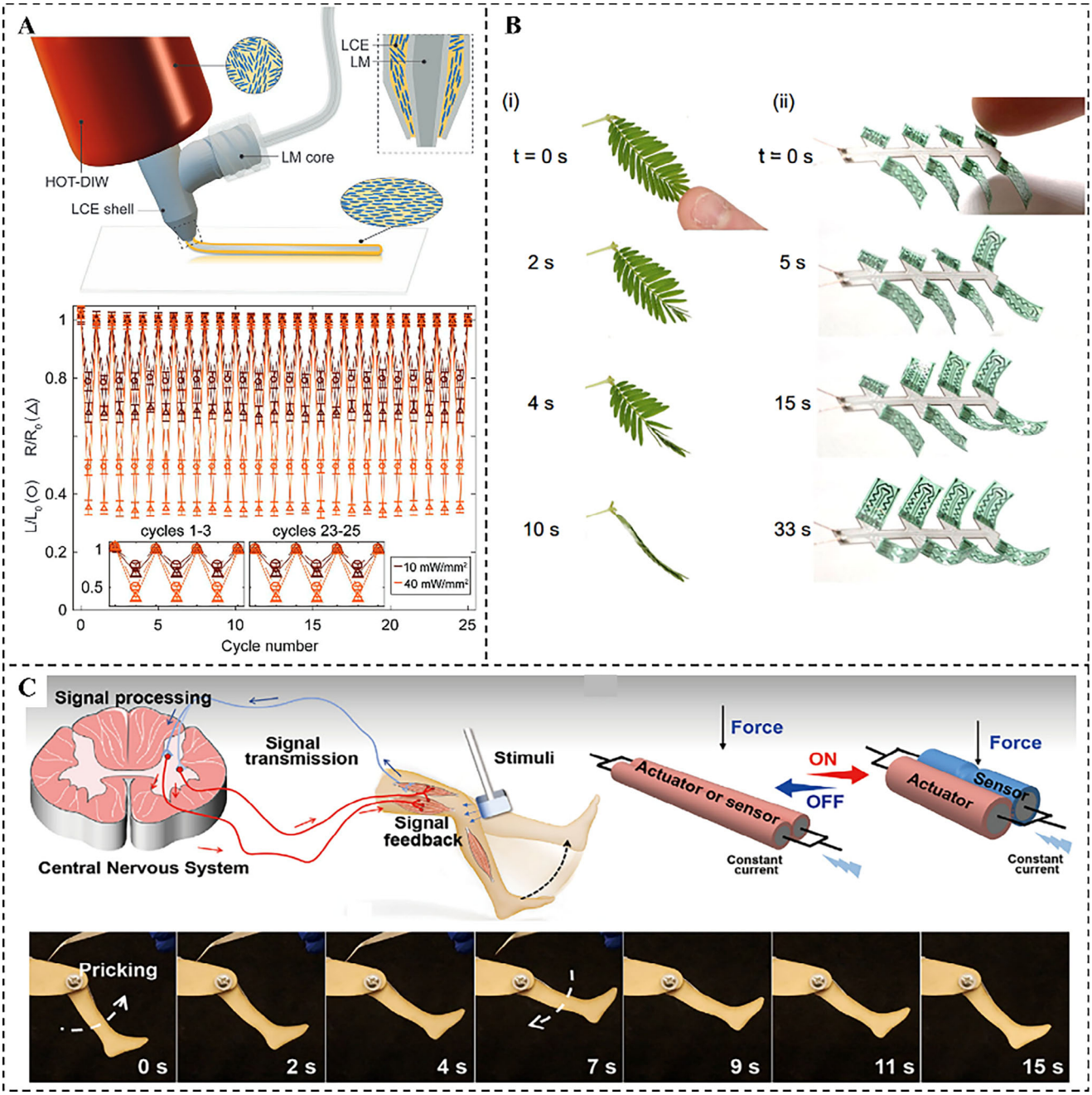

Figure 12. Applications of LCE actuators in sensing systems. A) Schematic of the 3D-printed iLCE fiber comprising a liquid metal core encapsulated by an LCE shell, along with the measured variations in normalized length (L/L_0) and resistance (R/R_0) under cyclic low- and high-power actuation (Reproduced with permission.[56] Copyright 2021, Elsevier). B) Comparison of the sequential leaf-folding behavior of a natural Mimosa pudica and its LCE-based biomimetic counterpart, activated by human touch (Reproduced with permission.[77] Copyright 2024, Springer Nature). C) An LCE-based artificial leg mimics a neuromuscular reflex arc, performing a knee-jerk response and kicking a wooden block upon external mechanical stimulation (Reproduced with permission.[152] Copyright 2024, Elsevier).

fundamental "high-stress–high-strain–fast-response" trade-off. Multiscale structural strategies—e.g., densely entangled or interpenetrating networks—offer a pathway to simultaneously improve strain, force, and power density, highlighting the potential of molecular–micro–macro integration for next-generation soft actuators.[174,175]

5.1.2. Actuation Rate

Thermally driven LCEs often show fast heating but slow cooling, limiting actuation frequency. Material-level strategies, such as adding thermally conductive fillers (graphene, metallic particles), combined with high surface-area or microchannel

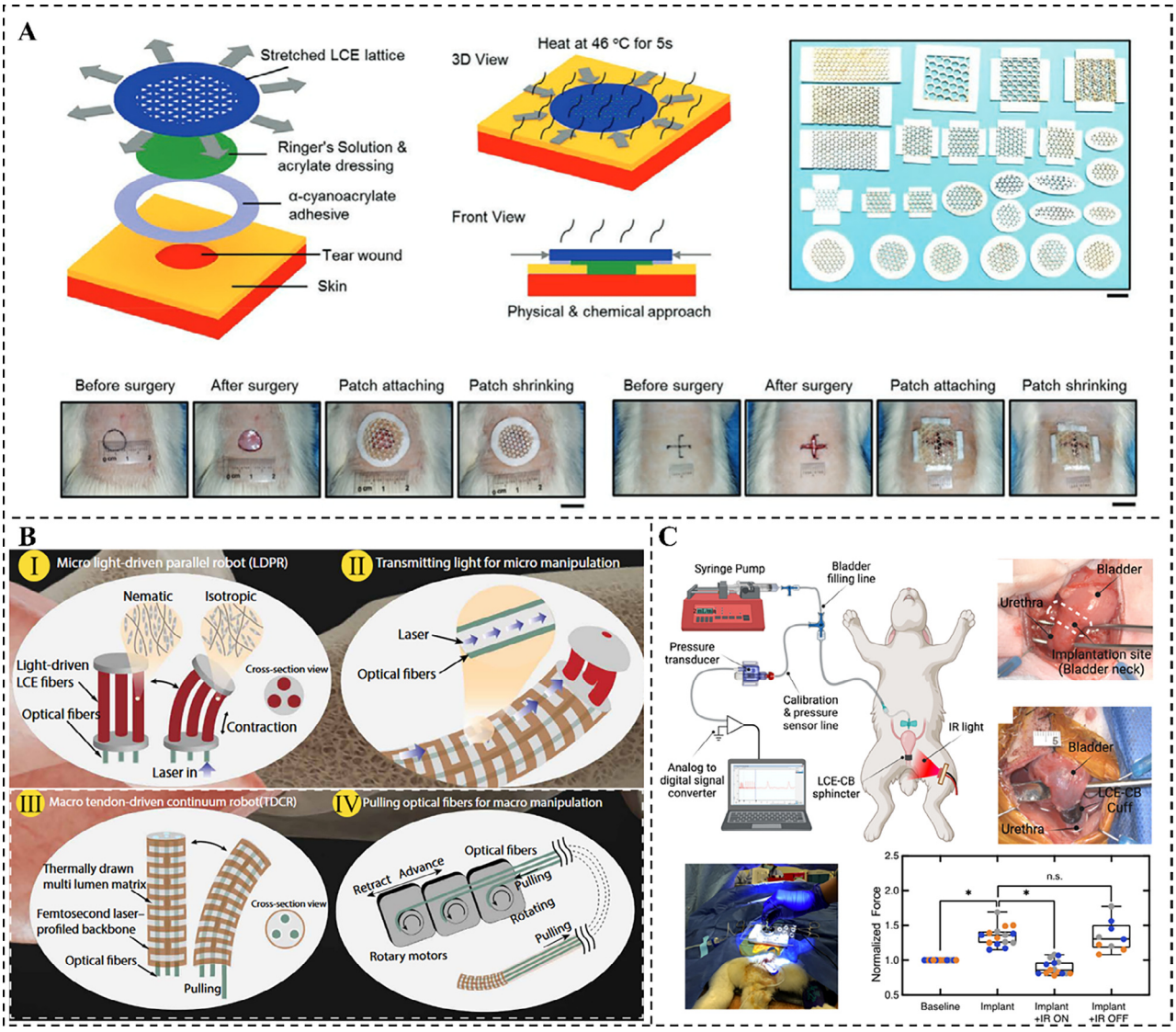

Figure 13. Applications of LCE actuators in biomedical fields. A) Schematic of the hemostatic treatment process using a contractile patch composed of an LCE-based metamaterial layer and an acrylate dressing. Upon stimulation, the LCE layer contracts biaxially to conform to irregular wounds, enabling sealing, hemostasis, and tissue regeneration (Reproduced with permission.[6] Copyright 2021, Wiley-VCH). B) Design and actuation of a sub-millimeter fiber robot with decoupled macro- and microscale motion capabilities. The robot integrates slender optical fibers to simultaneously enable tendon-driven macromotion and light-driven micromotion, achieving cross-scale operation (Reproduced with permission.[5] Copyright 2024, AAAS). C) Implanted LCE-carbon black (CB) cuff positioned around the bladder neck in multiparous rabbits, demonstrating controllable modulation of continence and unimpeded voiding under infrared illumination (Reproduced with permission.[173] Copyright 2023, Elsevier).

architectures, accelerate heat dissipation. System-level measures—lowering actuation temperature or incorporating active cooling (water-assisted, microfluidic, or thermoelectric)—further enhance cycle speed and stability.[36,101,161] Hierarchical integration of these strategies enables rapid, cyclic, and adaptive actuation, supporting high-performance intelligent soft actuators.

5.1.3. Material Stability

Long-term operation of LCE actuators is often limited by environmental stressors—thermal cycling, humidity, mechanical load, and oxidation—leading to fatigue and performance loss. Enhancing robustness begins with polymer network optimization. Incorporating dynamic sacrificial bonds, such as tetraarylsuccinonitrile (TASN), significantly improves fatigue resistance: LCE–TASN composites withstand thousands of 100% strain cycles and rapidly self-recover, demonstrating properties absent in conventional LCEs.[176]

Increasing crosslinking density and embedding nanofillers (e.g., CNTs, graphene, ceramics) further reinforce mechanical integrity, thermal stability, and resistance to photodegradation, extending operational lifespan.[150,177] By tuning microscopic crosslinking and filler networks alongside macroscopic architecture, LCEs achieve adaptive energy distribution and bioinspired

self-healing under multimodal stimuli. This multiscale strategy ensures stable actuation, high-frequency cycling durability, and reliable performance in soft devices and wearable systems.

5.2. Integrated Multifunctionality

Owing to their programmable shape-morphing and mechanical compliance, LCEs are ideal candidates for intelligent material systems. By coupling LCEs with flexible electronics, microcontrollers, and AI-driven algorithms, passive actuators can be upgraded into multifunctional devices with embedded sensing, feedback, and decision-making capabilities. Future developments may focus on closed-loop "sensing–decision–actuation" systems, enabling real-time monitoring, adaptive actuation, and autonomous operation under dynamic conditions–relevant to soft robotics, physiological signal tracking, and environmental signal integration.

The integration of machine learning, data-driven modeling, and advanced structural design allows real-time coupling of LCE deformation with multimodal signals, enabling life-like interactive behaviors, cross-scale motion, and self-regulating functions.[152,171,178] Further progress in robust feedback control, combined with energy harvesting and storage integration, could transform single LCE actuators into fully autonomous intelligent systems, unlocking new paradigms for soft robotics, wearable electronics, adaptive environments, and biomedical technologies.

5.3. Scalable and Controllable Fabrication

Despite exceptional laboratory performance, translating LCE actuators to industrial applications remains challenging, as fabrication strategies strongly influence actuation efficiency. Key obstacles include achieving precise alignment of liquid crystalline domains at scale, ensuring uniform precursor synthesis, controlling composition and stability, and reducing production costs. Most current LCE systems rely on small-batch, customized synthesis, limiting deployment in smart textiles, artificial muscles, medical devices, soft robotics, and morphing structures.

To enable industrial translation, advanced automated manufacturing technologies are needed, including high-resolution 3D/4D printing, high-speed fiber spinning, and continuous coating techniques.[73,128] For example, in high-speed fiber spinning, real-time monitoring of parameters such as fiber diameter, domain alignment, temperature, roller speed, pressure, and flow rate, combined with data-driven process optimization, allows precise, scalable, and reproducible production. Such approaches enhance consistency, reliability, and overall actuator performance, providing a practical pathway for large-scale deployment of LCE-based devices.

Acknowledgements

This work was supported by the National Natural Science Foundation of China (12 272 004).

Conflict of Interest

The authors declare no conflict of interest.

Data Availability Statement

All data necessary to evaluate the conclusions of the paper are provided in the paper.

Keywords

liquid crystal elastomers (LCEs), multifunctional applications, multiresponsive stimuli, soft actuators

Received: June 3, 2025
Revised: October 5, 2025
Published online: November 4, 2025

[1] D. Li, Y. Sun, X. Li, X. Li, Z. Zhu, B. Sun, S. Nong, J. Wu, T. Pan, W. Li, S. Zhang, M. Li, *ACS Nano* **2025**, *19*, 7075.
[2] X. Ma, P. Wang, L. Huang, R. Ding, K. Zhou, Y. Shi, F. Chen, Q. Zhuang, Q. Huang, Y. Lin, Z. Zheng, *Sci. Adv.* **2023**, *9*, adj2763.
[3] R. Kinjo, Y. Morimoto, B. Jo, S. Takeuchi, *Matter* **2024**, *7*, 948.
[4] J. Byun, M. Park, S.-M. Baek, J. Yoon, W. Kim, B. Lee, Y. Hong, K.-J. Cho, *Sci. Robot.* **2021**, *6*, abe0637.
[5] C. Zhou, Z. Xu, Z. Lin, X. Qin, J. Xia, X. Ai, C. Lou, Z. Huang, S. Huang, H. Liu, Y. Zou, W. Chen, G.-Z. Yang, A. Gao, *Sci. Adv.* **2024**, *10*, adr6428.
[6] J. Wu, S. Yao, H. Zhang, W. Man, Z. Bai, F. Zhang, X. Wang, D. Fang, Y. Zhang, *Adv. Mater.* **2021**, *33*, 2106175.
[7] Q. Cheng, W. Kang, H. Ma, Z. Wang, X. Liang, *Acta Mech. Sin.* **2025**, *41*, 424622.
[8] S. Ma, P. Xue, C. Valenzuela, X. Zhang, Y. Chen, Y. Liu, L. Yang, X. Xu, L. Wang, *Adv. Funct. Mater.* **2023**, *34*, 2309899.
[9] P. Liu, Z. Mao, Y. Zhao, J. Yin, C. Chu, X. Chen, J. Lu, *Adv. Sci.* **2024**, *11*, 2307830.
[10] G. Hou, X. Zhang, F. Du, Y. Wu, X. Zhang, Z. Lei, W. Lu, F. Zhang, G. Yang, H. Wang, Z. Liu, R. Wang, Q. Ge, J. Chen, G. Meng, N. X. Fang, X. Qian, *Nat. Nanotechnol.* **2023**, *19*, 77.
[11] J. Qiu, A. Ji, K. Zhu, Q. Han, W. Wang, Q. Qi, G. Chen, *Soft Rob.* **2023**, *10*, 713.
[12] Z. Ping, F. Xie, X. Gong, F. Zhang, J. Zheng, Y. Liu, J. Leng, *Adv. Funct. Mater.* **2024**, *34*, 2402592.
[13] J. Huang, L. Qiu, C. Ni, G. Chen, Q. Zhao, *Adv. Mater.* **2024**, *36*, 2408324.
[14] J.-H. Lee, S. Oh, I. Jeong, Y. J. Lee, M. C. Kim, J. S. Park, K. Hyun, T. H. Ware, S. Ahn, *Sci. Adv.* **2025**, *11*, adt7613.
[15] N. Qian, H. K. Bisoyi, M. Wang, S. Huang, Z. Liu, X. Chen, J. Hu, H. Yang, Q. Li, *Adv. Funct. Mater.* **2023**, *33*, 2214205.
[16] T. Wang, H.-J. Joo, S. Song, W. Hu, C. Keplinger, M. Sitti, *Sci. Adv.* **2023**, *9*, adg0292.
[17] X. Wang, S. Li, J.-C. Chang, J. Liu, D. Axinte, X. Dong, *Nat. Commun.* **2024**, *15*, 6296.
[18] T. J. K. Buchner, T. Fukushima, A. Kazemipour, S. Gravert, M. Prairie, P. Romanescu, P. Arm, Y. Zhang, X. Wang, S. L. Zhang, J. Walter, C. Keplinger, R. K. Katzschmann, *Nat. Commun.* **2024**, *15*, 7634.
[19] S. Xu, C. M. Nunez, M. Souri, R. J. Wood, *Sci. Robot.* **2023**, *8*, add4649.
[20] Z. Zheng, J. Han, Q. Shi, S. O. Demir, W. Jiang, M. Sitti, *Proc. Natl. Acad. Sci. U. S. A.* **2024**, *121*, 2320386121.
[21] Z. Ren, W. Hu, X. Dong, M. Sitti, *Nat. Commun.* **2019**, *10*, 2703.
[22] Z. Qi, M. Zhou, Y. Li, Z. Xia, W. Huo, X. Huang, *Adv. Mater. Technol.* **2021**, *6*, 2001124.
[23] Z. Nie, M. Wang, H. Yang, *Chem. Eur. J.* **2023**, *29*, 202301027.
[24] J. Gao, K. Wang, Y. Yang, W. Feng, *J. Mater. Chem. C* **2025**, *13*, 8425.

[25] L. T. De Haan, J. M. N. Verjans, D. J. Broer, C. W. M. Bastiaansen, A. P. H. J. Schenning, *J. Am. Chem. Soc.* **2014**, *136*, 10585.
[26] M. Chen, Y. Hou, R. An, H. J. Qi, K. Zhou, *Adv. Mater.* **2023**, *36*, 2303969.
[27] X. Tian, Y. Guo, J. Zhang, O. M. Ivasishin, J. Jia, J. Yan, *Small* **2024**, *20*, 2306952.
[28] M. Chen, M. Gao, L. Bai, H. Zheng, H. J. Qi, K. Zhou, *Adv. Mater.* **2023**, *35*, 2209566.
[29] Z. Guan, L. Wang, J. Bae, *Mater. Horiz.* **2022**, *9*, 1825.
[30] Y. Yao, A. M. Wilborn, B. Lemaire, F. Trigka, F. Stricker, A. H. Weible, S. Li, R. K. A. Bennett, T. C. Cheung, A. Grinthal, M. Zhernenkov, G. Freychet, P. Wąsik, B. Kozinsky, M. M. Lerch, X. Wang, J. Aizenberg, *Science* **2024**, *386*, 1161.
[31] W. Feng, A. Pal, T. Wang, Z. Ren, Y. Yan, Y. Lu, H. Yang, M. Sitti, *Adv. Funct. Mater.* **2023**, *33*, 2300731.
[32] Y. Zhang, Z. Wang, Y. Yang, Q. Chen, X. Qian, Y. Wu, H. Liang, Y. Xu, Y. Wei, Y. Ji, *Sci. Adv.* **2020**, *6*, aay8606.
[33] G. Chen, H. Feng, X. Zhou, F. Gao, K. Zhou, Y. Huang, B. Jin, T. Xie, Q. Zhao, *Nat. Commun.* **2023**, *14*, 6822.
[34] A. Cohen, D. Zarrouk, in *2020 IEEE/RSJ International Conference on Intelligent Robots and Systems (IROS)*, IEEE, Las Vegas, **2020**.
[35] C. Kim, K. Lee, S. Ryu, T. Seo, *IEEE/ASME Trans. Mechatron.* **2023**, *28*, 1836.
[36] M. Zadan, D. K. Patel, A. P. Sabelhaus, J. Liao, A. Wertz, L. Yao, C. Majidi, *Adv. Mater.* **2022**, *34*, 2200857.
[37] K. Liu, F. Hacker, C. Daraio, *Sci. Robot.* **2021**, *6*, abf5116.
[38] Z. Nie, M. Wang, S. Huang, Z. Liu, H. Yang, *Angew. Chem., Int. Ed.* **2023**, *62*, 202304081.
[39] D. J. Roach, C. Yuan, X. Kuang, V. C.-F. Li, P. Blake, M. L. Romero, I. Hammel, K. Yu, H. J. Qi, *ACS Appl. Mater. Interfaces* **2019**, *11*, 19514.
[40] J. Ma, Z. Yang, *Matter* **2025**, *8*, 101950.
[41] L. Ren, Y. He, B. Wang, J. Xu, Q. Wu, Z. Wang, W. Li, L. Ren, X. Zhou, Q. Liu, B. Li, Z. Song, *Adv. Funct. Mater.* **2024**, *34*, 2400161.
[42] Y. Wang, H. Xuan, L. Zhang, H. Huang, R. E. Neisiany, H. Zhang, S. Gu, Q. Guan, Z. You, *Adv. Mater.* **2024**, *36*, 2313761.
[43] M. O. Saed, C. P. Ambulo, H. Kim, R. De, V. Raval, K. Searles, D. A. Siddiqui, J. M. O. Cue, M. C. Stefan, M. R. Shankar, T. H. Ware, *Adv. Funct. Mater.* **2019**, *29*, 1806412.
[44] P. Sartori, R. S. Yadav, J. Del Barrio, A. DeSimone, C. Sánchez-Somolinos, *Adv. Sci.* **2024**, *11*, 2308561.
[45] Z. Wang, Z. Wang, Y. Zheng, Q. He, Y. Wang, S. Cai, *Sci. Adv.* **2020**, *6*, abc0034.
[46] F. Zhai, Y. Feng, Z. Li, Y. Xie, J. Ge, H. Wang, W. Qiu, W. Feng, *Matter* **2021**, *4*, 3313.
[47] X. Yang, C. Valenzuela, X. Zhang, Y. Chen, Y. Yang, L. Wang, W. Feng, *Matter* **2023**, *6*, 1278.
[48] R. Telles, J. A. Mancini, J. Barrera, M. Simoes, D. H. Porcincula, A. Bischoff, D. J. Roach, S. C. Leguizamon, E. Lee, C. C. Cook, J. A. Lewis, *Adv. Mater.* **2025**, *37*, 2420048.
[49] X. Feng, L. Wang, Z. Xue, C. Xie, J. Han, Y. Pei, Z. Zhang, W. Guo, B. Lu, *Sci. Adv.* **2024**, *10*, adk3854.
[50] J. Tian, C. Shi, G. Nie, C. Li, Y. Zhao, *Adv. Sci.* **2025**, *12*, 07922.
[51] T. Hessberger, L. Braun, R. Zentel, *Polymers* **2016**, *8*, 410.
[52] M. Patel, A. Alvarez-Fernandez, M. J. Fornerod, A. N. P. Radhakrishnan, A. Taylor, S. Ten Chua, S. Vignolini, B. Schmidt-Hansberg, A. Iles, S. Guldin, *ACS Omega* **2023**, *8*, 20404.
[53] D. Ditter, P. Blümler, B. Klöckner, J. Hilgert, R. Zentel, *Adv. Funct. Mater.* **2019**, *29*, 1902454.
[54] Y. Wang, J. Sun, W. Liao, Z. Yang, *Adv. Mater.* **2022**, *34*, 2107840.
[55] W. Liao, Z. Yang, *Adv. Mater. Technol.* **2022**, *7*, 2101260.
[56] A. Kotikian, J. M. Morales, A. Lu, J. Mueller, Z. S. Davidson, J. W. Boley, J. A. Lewis, *Adv. Mater.* **2021**, *33*, 2101814.
[57] B. Ma, C. Xu, L. Cui, C. Zhao, H. Liu, *ACS Appl. Mater. Interfaces* **2021**, *13*, 5574.
[58] T. Zhao, Y. Zhang, Y. Fan, J. Wang, H. Jiang, J. Lv, *J. Mater. Chem. C* **2022**, *10*, 3796.
[59] G. Chen, B. Ma, Y. Chen, Y. Chen, J. Zhang, H. Liu, *Adv. Sci.* **2024**, *11*, 2306129.
[60] D. J. Roach, X. Sun, X. Peng, F. Demoly, K. Zhou, H. J. Qi, *Adv. Funct. Mater.* **2022**, *32*, 2203236.
[61] H. Zeng, O. M. Wani, P. Wasylczyk, R. Kaczmarek, A. Priimagi, *Adv. Mater.* **2017**, *29*, 1701814.
[62] L. Xu, C. Zhu, S. C. Lamont, R. Tao, Y. Mao, Z. Guan, L. Zhang, J. Ding, F. J. Vernerey, *Adv. Funct. Mater.* **2025**, *35*, 2424033.
[63] Y. Zhu, J. Huang, H. Mi, Z. Xu, Y. Ai, S. Gong, C. Li, M. Wang, L. Chen, *Angew. Chem., Int. Ed.* **2025**, *64*, 202421915.
[64] Y. Tang, F. Pan, L. Qin, Y. Yu, *Adv. Funct. Mater.* **2025**, *35*, 2506987.
[65] Q. He, Z. Wang, Y. Wang, A. Minori, M. T. Tolley, S. Cai, *Sci. Adv.* **2019**, *5*, aax5746.
[66] C. P. Ambulo, J. J. Burroughs, J. M. Boothby, H. Kim, M. R. Shankar, T. H. Ware, *ACS Appl. Mater. Interfaces* **2017**, *9*, 37332.
[67] J. A. Herman, R. Telles, C. C. Cook, S. C. Leguizamon, J. A. Lewis, B. Kaehr, T. J. White, D. J. Roach, *Adv. Mater.* **2024**, *36*, 2414209.
[68] X. Huang, L. Qin, J. Wang, X. Zhang, B. Peng, Y. Yu, *Adv. Funct. Mater.* **2022**, *32*, 2208312.
[69] D. S. Kim, Y.-J. Lee, Y. B. Kim, Y. Wang, S. Yang, *Sci. Adv.* **2023**, *9*, adh5107.
[70] H. Liang, Y. Zhang, E. He, Y. Yang, Y. Liu, H. Xu, Z. Yang, Y. Wang, Y. Wei, Y. Jii, *Adv. Mater.* **2024**, *36*, 2400286.
[71] H. Yang, X. Yin, C. Zhang, B. Chen, P. Sun, Y. Xu, *Sci. Adv.* **2025**, *11*, ads3058.
[72] A. Kotikian, A. A. Watkins, G. Bordiga, A. Spielberg, Z. S. Davidson, K. Bertoldi, J. A. Lewis, *Adv. Mater.* **2024**, *36*, 2310743.
[73] W. Hou, J. Wang, J. Lv, *Adv. Mater.* **2023**, *35*, 2211800.
[74] S. Wu, Y. Hong, Y. Zhao, J. Yin, Y. Zhu, *Sci. Adv.* **2023**, *9*, adf8014.
[75] Q. He, Z. Wang, Y. Wang, Z. Wang, C. Li, R. Annapooranan, J. Zeng, R. Chen, S. Cai, *Sci. Robot.* **2021**, *6*, abi9704.
[76] J. Forman, O. Kilic Afsar, S. Nicita, R. H.-J. Lin, L. Yang, M. Hofmann, A. Kothakonda, Z. Gordon, C. Honnet, K. Dorsey, N. Gershenfeld, H. Ishii, in *Proceedings of the 36th Annual ACM Symposium on User Interface Software and Technology*, ACM, San Francisco, **2023**.
[77] P. Lyu, D. J. Broer, D. Liu, *Nat. Commun.* **2024**, *15*, 4191.
[78] W. Feng, D. J. Broer, D. Liu, *Adv. Funct. Mater.* **2020**, *30*, 1901681.
[79] L. Xu, C. Zhu, S. Lamont, X. Zou, Y. Yang, S. Chen, J. Ding, F. J. Vernerey, *Soft Rob.* **2024**, *11*, 464.
[80] Y. Xiao, Z. Jiang, X. Tong, Y. Zhao, *Adv. Mater.* **2019**, *31*, 1903452.
[81] C. Wang, K. Sim, J. Chen, H. Kim, Z. Rao, Y. Li, W. Chen, J. Song, R. Verduzco, C. Yu, *Adv. Mater.* **2018**, *30*, 1706695.
[82] L. Yang, Y. Liu, R. Bi, Y. Chen, C. Valenzuela, Y. Yang, H. Liu, L. Wang, W. Feng, *Adv. Funct. Mater.* **2025**, *35*, 2504979.
[83] Y. Wu, S. Zhang, Y. Yang, Z. Li, Y. Wei, Y. Ji, *Sci. Adv.* **2022**, *8*, abo6021.
[84] Z. Wang, M. Si, J. Han, Y. Shen, G. Yin, K. Yin, P. Xiao, T. Chen, *Angew. Chem., Int. Ed.* **2025**, *64*, 202416095.
[85] F. Qi, Y. Li, Y. Hong, Y. Zhao, H. Qing, J. Yin, *Proc. Natl. Acad. Sci. U. S. A.* **2024**, *121*, 2312680121.
[86] Y. Zhao, Y. Hong, F. Qi, Y. Chi, H. Su, J. Yin, *Adv. Mater.* **2023**, *35*, 2207372.
[87] Q. Liu, Z. Jiang, X. Jiang, J. Zhao, Y. Zhang, Y. Liu, J. Hou, Y. Xiao, W. Pu, Y. Zhao, *Angew. Chem., Int. Ed.* **2025**, *64*, 202500527.
[88] H. Liu, H. Tian, X. Li, X. Chen, K. Zhang, H. Shi, C. Wang, J. Shao, *Sci. Adv.* **2022**, *8*, abn5722.
[89] W. Feng, L. Chu, M. B. De Rooij, D. Liu, D. J. Broer, *Adv. Sci.* **2021**, *8*, 2004051.
[90] Z. Kuang, J. Liu, W. Meng, T. Ikeda, J. Wang, L. Jiang, *Adv. Funct. Mater.* **2024**, *35*, 2421111.
[91] M. Yang, Y. Xu, X. Zhang, H. K. Bisoyi, P. Xue, Y. Yang, X. Yang, C. Valenzuela, Y. Chen, L. Wang, W. Feng, Q. Li, *Adv. Funct. Mater.* **2022**, *32*, 2201884.

[92] J. Ma, Y. Wang, J. Sun, Z. Yang, *Adv. Funct. Mater.* **2024**, *34*, 2402403.
[93] W. Liao, Z. Yang, *Mater. Horiz.* **2023**, *10*, 576.
[94] K. Kim, Y. Guo, J. Bae, S. Choi, H. Y. Song, S. Park, K. Hyun, S. Ahn, *Small* **2021**, *17*, 2100910.
[95] T. Tang, S. Alfarhan, K. Jin, X. Li, *Adv. Funct. Mater.* **2023**, *33*, 2211602.
[96] M. Del Pozo, L. Liu, M. Pilz Da Cunha, D. J. Broer, A. P. H. J. Schenning, *Adv. Funct. Mater.* **2020**, *30*, 2005560.
[97] H. Guo, T. Ruoko, H. Zeng, A. Priimagi, *Adv. Funct. Mater.* **2023**, *34*, 2312068.
[98] G. Chen, B. Jin, Y. Shi, Q. Zhao, Y. Shen, T. Xie, *Adv. Mater.* **2022**, *34*, 2201679.
[99] B. Jin, J. Liu, Y. Shi, G. Chen, Q. Zhao, S. Yang, *Adv. Mater.* **2022**, *34*, 2107855.
[100] M. López-Valdeolivas, D. Liu, D. J. Broer, C. Sánchez-Somolinos, *Macromol. Rapid Commun.* **2018**, *39*, 1700710.
[101] Y. Zhao, Q. Li, Z. Liu, Y. Alsaid, P. Shi, M. Khalid Jawed, X. He, *Sci. Rob.* **2023**, *8*, adf4753.
[102] Y. Wang, R. Yin, L. Jin, M. Liu, Y. Gao, J. Raney, S. Yang, *Adv. Funct. Mater.* **2023**, *33*, 2210614.
[103] Y. Wang, Q. Guan, D. Lei, R. E. Neisiany, Y. Guo, S. Gu, Z. You, *ACS Nano* **2022**, *16*, 19393.
[104] H. Yu, T. Ikeda, *Adv. Mater.* **2011**, *23*, 2149.
[105] J. Gao, M. Tian, Y. He, H. Yi, J. Guo, *Adv. Funct. Mater.* **2022**, *32*, 2107145.
[106] Y. Yu, T. Maeda, J. Mamiya, T. Ikeda, *Angew. Chem., Int. Ed.* **2007**, *119*, 899.
[107] T. Ikeda, J. Mamiya, Y. Yu, *Angew. Chem., Int. Ed.* **2007**, *46*, 506.
[108] V. Maurin, Y. Chang, Q. Ze, S. Leanza, J. Wang, R. R. Zhao, *Adv. Mater.* **2024**, *36*, 2302765.
[109] J. Lee, J. Bae, J. H. Hwang, M. Choi, Y. S. Kim, S. Park, J. Na, D. Kim, S. Ahn, *Adv. Funct. Mater.* **2022**, *32*, 2110360.
[110] H. Jiang, C. Chung, M. L. Dunn, K. Yu, *Nat. Commun.* **2024**, *15*, 8491.
[111] C. P. Ambulo, M. J. Ford, K. Searles, C. Majidi, T. H. Ware, *ACS Appl. Mater. Interfaces* **2021**, *13*, 12805.
[112] H. Kim, J. A. Lee, C. P. Ambulo, H. B. Lee, S. H. Kim, V. V. Naik, C. S. Haines, A. E. Aliev, R. Ovalle-Robles, R. H. Baughman, T. H. Ware, *Adv. Funct. Mater.* **2019**, *29*, 1905063.
[113] J. Liu, Y. Gao, H. Wang, R. Poling-Skutvik, C. O. Osuji, S. Yang, *Adv. Intell. Syst.* **2020**, *2*, 1900163.
[114] D. Wu, Y. Zhang, H. Yang, A. Wei, Y. Zhang, A. Mensah, R. Yin, P. Lv, Q. Feng, Q. Wei, *Mater. Horiz.* **2023**, *10*, 2587.
[115] H. Shin, W. Jeong, T. H. Han, *Nat. Commun.* **2024**, *15*, 10507.
[116] Y. Sun, L. Wang, Z. Zhu, X. Li, H. Sun, Y. Zhao, C. Peng, J. Liu, S. Zhang, M. Li, *Adv. Mater.* **2023**, *35*, 2302824.
[117] J. Lub, D. J. Broer, N. Van Den Broek, *Liebigs Ann./ Recl.* **1997**, *1997*, 2281.
[118] H. Yang, A. Buguin, J.-M. Taulemesse, K. Kaneko, S. Méry, A. Bergeret, P. Keller, *J. Am. Chem. Soc.* **2009**, *131*, 15000.
[119] E.-K. Fleischmann, F. R. Forst, K. Köder, N. Kapernaum, R. Zentel, *J. Mater. Chem. C* **2013**, *1*, 5885.
[120] A. Kotikian, C. McMahan, E. C. Davidson, J. M. Muhammad, R. D. Weeks, C. Daraio, J. A. Lewis, *Sci. Rob.* **2019**, *4*, aax7044.
[121] X. Yang, S. Leanza, Q. Ze, R. R. Zhao, *Mater. Today* **2025**, *87*, 11.
[122] J. Jeon, J.-C. Choi, H. Lee, W. Cho, K. Lee, J. G. Kim, J.-W. Lee, K.-I. Joo, M. Cho, H.-R. Kim, J. J. Wie, *Mater. Today* **2021**, *49*, 97.
[123] W. Zou, X. Lin, E. M. Terentjev, *Adv. Mater.* **2021**, *33*, 2101955.
[124] Y. Xia, X. Zhang, S. Yang, *Angew. Chem., Int. Ed.* **2018**, *57*, 5665.
[125] C. M. Yakacki, M. Saed, D. P. Nair, T. Gong, S. M. Reed, C. N. Bowman, *RSC Adv.* **2015**, *5*, 18997.
[126] A. M. Martinez, M. K. McBride, T. J. White, C. N. Bowman, *Adv. Funct. Mater.* **2020**, *30*, 2003150.
[127] J. Sun, W. Liao, Z. Yang, *Adv. Mater.* **2023**, *35*, 2302706.
[128] A. P. Martinez, L. K. Decker, K. Wang, J. B. Kim, C. B. Murray, S. Yang, *Adv. Funct. Mater.* **2024**, *34*, 2422176.
[129] A. P. Martinez, A. Ng, S. H. Nah, S. Yang, *Adv. Funct. Mater.* **2024**, *34*, 2400742.
[130] Y. Wang, W. Liao, J. Sun, R. Nandi, Z. Yang, *Adv. Mater. Technol.* **2022**, *7*, 2100934.
[131] Q. Wang, X. Tian, D. Zhang, Y. Zhou, W. Yan, D. Li, *Nat. Commun.* **2023**, *14*, 3869.
[132] S. Li, H. Bai, Z. Liu, X. Zhang, C. Huang, L. W. Wiesner, M. Silberstein, R. F. Shepherd, *Sci. Adv.* **2021**, *7*, abg3677.
[133] C. D. Hasson, F. J. Davis, G. R. Mitchell, *Mol. Cryst. Liq. Cryst.* **1999**, *332*, 155.
[134] M. Devetak, B. Zupančič, A. Lebar, P. Umek, B. Zalar, V. Domenici, G. Ambrožič, M. Žigon, M. Čopič, I. Drevenšek-Olenik, *Phys. Rev. E* **2009**, *80*, 050701.
[135] T. H. Ware, M. E. McConney, J. J. Wie, V. P. Tondiglia, T. J. White, *Science* **2015**, *347*, 982.
[136] D. Ditter, W.-L. Chen, A. Best, H. Zappe, K. Koynov, C. K. Ober, R. Zentel, *J. Mater. Chem. C* **2017**, *5*, 12635.
[137] T. J. White, D. J. Broer, *Nat. Mater.* **2015**, *14*, 1087.
[138] J. Küpfer, H. Finkelmann, *Macromol. Rapid Commun.* **1991**, *12*, 717.
[139] Y. Xiao, Z. Jiang, L. Yin, J. Jiang, Y. Zhao, *J. Mater. Chem. C* **2021**, *9*, 16566.
[140] W. Feng, D. J. Broer, D. Liu, *Adv. Mater.* **2018**, *30*, 1704970.
[141] D. Liu, D. J. Broer, *Angew. Chem., Int. Ed.* **2014**, *53*, 4542.
[142] D. Liu, L. Liu, P. R. Onck, D. J. Broer, *Proc. Natl. Acad. Sci. U. S. A.* **2015**, *112*, 3880.
[143] N. A. Traugutt, D. Mistry, C. Luo, K. Yu, Q. Ge, C. M. Yakacki, *Adv. Mater.* **2020**, *32*, 2000797.
[144] A. Kotikian, R. L. Truby, J. W. Boley, T. J. White, J. A. Lewis, *Adv. Mater.* **2018**, *30*, 1706164.
[145] J. Küupfer, H. Finkelmann, *Macromol. Chem. Phys.* **1994**, *195*, 1353.
[146] H. Finkelmann, H. Kock, G. Rehage, *Makromol. Chem., Rapid Commun.* **1981**, *2*, 317.
[147] Y. Yu, M. Nakano, T. Ikeda, *Nature* **2003**, *425*, 145.
[148] M. Yamada, M. Kondo, J. Mamiya, Y. Yu, M. Kinoshita, C. J. Barrett, T. Ikeda, *Angew. Chem., Int. Ed.* **2008**, *47*, 4986.
[149] A. Kaiser, M. Winkler, S. Krause, H. Finkelmann, A. M. Schmidt, *J. Mater. Chem.* **2009**, *19*, 538.
[150] L. Yang, K. Setyowati, A. Li, S. Gong, J. Chen, *Adv. Mater.* **2008**, *20*, 2271.
[151] W. Pang, S. Xu, J. Wu, R. Bo, T. Jin, Y. Xiao, Z. Liu, F. Zhang, X. Cheng, K. Bai, H. Song, Z. Xue, L. Wen, Y. Zhang, *Proc. Natl. Acad. Sci. U. S. A.* **2022**, *119*, 2215028119.
[152] Y. Chen, C. Valenzuela, Y. Liu, X. Yang, Y. Yang, X. Zhang, S. Ma, R. Bi, L. Wang, W. Feng, *Matter* **2024**, *8*, 101904.
[153] S. Xu, X. Hu, R. Yang, C. Zang, L. Li, Y. Xiao, W. Liu, B. Tian, W. Pang, R. Bo, Q. Liu, Y. Yang, Y. Lai, J. Wu, H. Zhao, L. Wen, Y. Zhang, *Nat. Mach. Intell.* **2025**, *7*, 703.
[154] M. Wu, X. Zhou, J. Zhang, L. Liu, S. Wang, L. Zhu, Z. Ming, Y. Zhang, Y. Xia, W. Li, Z. Zhou, M. Fan, J. Xiong, *Adv. Mater.* **2024**, *36*, 2409606.
[155] Y. Zhao, Y. Chi, Y. Hong, Y. Li, S. Yang, J. Yin, *Proc. Natl. Acad. Sci. U. S. A.* **2022**, *119*, 2200265119.
[156] Z.-C. Jiang, Q. Liu, Y.-Y. Xiao, Y. Zhao, *Prog. Polym. Sci.* **2024**, *153*, 101829.
[157] Z. Deng, K. Li, A. Priimagi, H. Zeng, *Nat. Mater.* **2024**, *23*, 1728.
[158] Y. Zhao, Y. Hong, Y. Li, F. Qi, H. Qing, H. Su, J. Yin, *Sci. Adv.* **2023**, *9*, adi3254.
[159] C. Liu, K. Li, X. Yu, J. Yang, Z. Wang, *Adv. Mater.* **2024**, 2314093.
[160] C. Li, J. Li, X. Yi, *ACS Appl. Mater. Interfaces* **2025**, *17*, 47456.
[161] Y. Zhao, Z. Liu, P. Shi, C. Chen, Y. Alsaid, Y. Yan, X. He, *Nat. Mater.* **2024**, *24*, 116.
[162] Z. Jiang, B. B. A. Abbasi, S. Aloko, F. Mokhtari, G. M. Spinks, *Adv. Mater.* **2023**, *35*, 2210419.
[163] Z. Yang, J. Li, X. Chen, Y. Fan, J. Huang, H. Yu, S. Yang, E. Chen, *Adv. Mater.* **2023**, *35*, 2211648.

[164] W. Chen, D. Tong, L. Meng, B. Tan, R. Lan, Q. Zhang, H. Yang, C. Wang, K. Liu, *Adv. Mater.* **2024**, *36*, 2400763.
[165] B. Cui, M. Ren, L. Dong, Y. Wang, J. He, X. Wei, Y. Zhao, P. Xu, X. Wang, J. Di, Q. Li, *ACS Nano* **2023**, *17*, 12809.
[166] S. Leanza, J. Lu-Yang, B. Kaczmarski, S. Wu, E. Kuhl, R. R. Zhao, *Adv. Funct. Mater.* **2024**, *34*, 2400396.
[167] L. Albaugh, S. Hudson, L. Yao, in *Proceedings of the 2019 CHI Conference on Human Factors in Computing Systems*, ACM, Glasgow, Scotland **2019**.
[168] P. E. S. Silva, X. Lin, M. Vaara, M. Mohan, J. Vapaavuori, E. M. Terentjev, *Adv. Mater.* **2023**, *35*, 2210689.
[169] Y. Zhang, X. Zhou, L. Liu, S. Wang, Y. Zhang, M. Wu, Z. Lu, Z. Ming, J. Tao, J. Xiong, *Adv. Mater.* **2024**, *36*, 2404696.
[170] L. Zhang, S. Xing, H. Yin, H. Weisbecker, H. T. Tran, Z. Guo, T. Han, Y. Wang, Y. Liu, Y. Wu, W. Xie, C. Huang, W. Luo, M. Demaesschalck, C. McKinney, S. Hankley, A. Huang, B. Brusseau, J. Messenger, Y. Zou, W. Bai, *Nat. Commun.* **2024**, *15*, 4777.
[171] S. A. M. Weima, R. Norouzikudiani, J. Baek, J. A. Peixoto, T. K. Slot, D. J. Broer, A. DeSimone, D. Liu, *Sci. Adv.* **2024**, *10*, adp0421.
[172] T. Zang, J. Wang, G. Yan, X. Lu, J. Hu, H. Xia, Y. Zhao, *Adv. Mater.* **2025**, *37*, 08694.
[173] S. Tasmim, Z. Yousuf, F. S. Rahman, E. Seelig, A. J. Clevenger, S. N. VandenHeuvel, C. P. Ambulo, S. Raghavan, P. E. Zimmern, M. I. Romero-Ortega, T. H. Ware, *Biomaterials* **2023**, *292*, 121912.
[174] H.-F. Lu, M. Wang, X.-M. Chen, B.-P. Lin, H. Yang, *J. Am. Chem. Soc.* **2019**, *141*, 14364.
[175] C. Li, T. Liu, Y. Li, L. Wang, R. Cheng, J. Ding, Z. Yang, A. Xing, K. Wang, M. Ren, Y. Su, L. Zhu, Q. Lin, *Adv. Mater.* **2025**, *37*, 13876.
[176] Y. Zhu, M. Wang, J. Huang, H. Mi, Z. Xu, F. Wu, L. Chen, H. Yang, Y. Chen, *Macromolecules* **2024**, *57*, 8329.
[177] M. Wang, X. Li, Y. Gai, Y. Luo, H. Yang, *Adv. Mater.* **2025**, *37*, 2506129.
[178] J. Cho, M. Lee, T. Park, Y. Wang, H. Lee, S. Cai, Y. Park, *Adv. Mater.* **2025**, *37*, 03094.

Chenglin Li is a Ph.D. student at Peking University. His research focuses on the design and fabrication of multifunctional actuators based on liquid crystal elastomers.

Jing Li is a Ph.D. student at Peking University. Her research focuses on the mechanics and design of mechanical metamaterials based on bistable structures.

Huiling Duan is a Boya Chair Professor, founding Director of the Faculty of Engineering, and Dean of the College of Engineering at Peking University. Her research focuses on interface mechanics and fluid-structure interactions. She has been elected as a member of the Chinese Academy of Sciences and an International Fellow of the Canadian Academy of Engineering. Currently, she holds several key academic leadership roles, including serving on the IUTAM Symposia Panel for Solid Mechanics, as Vice President of the Chinese Society of Theoretical and Applied Mechanics, and as Vice President of the China Women's Association for Science and Technology.

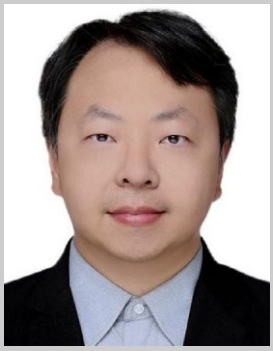

Xin Yi is an Associate Professor at Peking University. He earned his Ph.D. in Solid Mechanics from Brown University in 2014. Professor Yi's research focuses on the nonlinear mechanics of soft engineering and biological interfaces, as well as the mechanical behavior and additive manufacturing of high-performance metallic materials.